AGH University of Science and Technology

DEPARTAMENT OF POWER ELECTRONICS AND ENERGY CONTROL SYSTEMS

FACULTY OF ELECTRYCAL ENGINEERING, AUTOMATICS, COMPUTER SCIENCE AND BIOMEDICAL

Autoreferat rozprawy doktorskiej

M. Sc. Chamberlin Stéphane Azebaze Mboving

Methods for Reducing Voltage and Current Distortion Caused by Power Electronic Converters in Power Systems

Metody redukcji odkształcenia napięć i prądów powodowanych przez przekształtniki energoelektroniczne w sieciach elektroenergetycznych

Supervisor:
prof. dr hab. inż. Zbigniew Hanzelka

Co-supervisor:
dr inż. Ryszard Klempka

CRACOW 2020

1. Wstęp

Energia elektryczna jest towarem i dbanie o jej jakość jest niezbędne. Zaburzenia jakości dostawy energii elektrycznej są liczne i różnorodne (spadki i wzrosty napięcia, wahania, odkształcenie itp.), co oznacza, że stosuje się wiele metod, żeby redukować ich poziom w systemie elektroenergetycznym. Niniejsza praca koncentruje się na łagodzeniu zaburzeń, takich jak asymetria, harmoniczne i compensacji moc bierna podstawowej harmoniczne, stosując do tego celu filtry pasywne, aktywne i hybrydowe.

Celem pracy jest zaprojektowanie hybrydowego filtru aktywnego, który jest połączeniem filtru aktywnego z filtrem pasywnym. W celu skutecznego zaprojektowania takiego filtru, w niniejszej pracy przedstawiono szczegółową analizę (symulacja i badania laboratoryjne) różnych struktur filtrów aktywnych i pasywnych.

Rozpatrywane są następujące struktury filtru pasywnego: równoległy (prosty), szeregowy, podwójnie nastrojony, szerokopasmowe (pierwszego, drugiego i trzeciego rzędu oraz typu C), a także hybrydowy filtr pasywny. Każdy z nich jest indywidualnie analizowany pod kątem charakterystyki impedancji w funkcji częstotliwości oraz wpływu zjawiska odstrojenia i rezystancji tłumienia na ich efektywność. Porównano niektóre struktury filtru pasywnego (grupa dwóch filtrów prostych & filtr podwójnie nastrojony, szeregowy filtr pasywny i hybrydowy filtr pasywny), a także metody podziału całkowitej mocy biernej w grupie filtrów. Wyniki symulacyjne zostały potwierdzone badaniami w laboratorium następujących struktur filtru pasywnego: filtr prosty, grupa dwóch filtrów prostych, filtry pierwszego i drugiego rzędu.

W niniejszej pracy analizowano równoległy filtr aktywny – trójfazowy, trójprzewodowy. Celem jego stosowania jest kompensacja asymetrii i odkształcenia napięcia oraz mocy biernej podstawowej harmonicznej przy użyciu oryginalnego algorytmu sterowania - opartego na teorii *p-q* - zaproponowanego przez autora. W pracy uwzględniono badania wpływu dławików: włączonego między PWP a sieć zasilającą, wejściowego prostownika, wejściowego równoległego filtru aktywnego oraz kondensatora strony DC na efektywność działania filtru. Eksperymenty laboratoryjne równoległego filtru aktywnego - potwierdzające wyniki badań symulacyjnych - zostały przeprowadzane z wykorzystaniem struktury czteroprzewodowej z dzieloną pojemnością po stronie DC.

Po szczegółowych badaniach filtru pasywnego i aktywnego, w następnej kolejności zostały przeanalizowane struktury hybrydowe filtru aktywnego: model równoległego filtru aktywnego (trójfazowy, trzygałęziowy) połączonego szeregowo z filtrem prostym (badania symulacyjne) i model równoległego filtru aktywnego (czteroprzewodowy z dzieloną pojemnością od strony DC) połączony równolegle z grupą dwóch filtrów prostych (badania laboratoryjne). Autor zaproponował oryginalny algorytm sterowania oparty na teorii mocy *p-q* dla tej struktury.

2. Thesis, objective and scope of work

The growing number and unit power of non-linear load and electrical energy sources has forced the development and use of different technical solutions intended to reduce current and voltage distortion. Except for the passive methods, the active filtration and reactive power compensation systems are gaining more and more popularity. In their case, one of the highlighted disadvantages stills high price, especially in the systems with high power intended for use in medium or high voltage networks. However, it is possible to use the advantages of both solutions - passive and active. Such of systems are hybrid structures allowing to obtain the desired filtration effect and compensation of reactive power at moderate costs.

To build an effective hybrid filtration system, thorough knowledge of the *LC* filters frequency characteristics as well as active filters control algorithms are needed. The aim of the work was to acquire and present such knowledge by analyzing a very large number of different cases. Thanks to this, it was possible to formulate generalizing conclusions as a set of rules useful in the practice of designing such systems. Demonstrating that having such knowledge gives the opportunity to use the advantages of both components - passive and active, and allows to avoid the design errors is the main thesis that the author tried to prove in this work.

The performance of passive harmonic filtration and reactive power compensation systems was analyzed in great detail. The sensitivity of the effectiveness of their work in response to the change in the value of their elements was examined as well as the impact of the power supply network and the parameters of the filtered/compensated load were analyzed. Theoretical and simulation considerations were confirmed by laboratory tests.

In the next parts of the work, the designed model of the active power filter electronic converter and its control system were checked in simulation tests. As in the case of passive filters, the impact of various factors on the active filter work efficiency was analyzed. The selected aspects of theoretical considerations were supplemented by studies on the physical model in the laboratory conditions.

In the final part of the thesis, the passive and active systems were combined into a very rarely considered hybrid structure and the advantages of such of solution were confirmed by simulation.

3. Simulation analyzis

The simulation studies were performed in MATLAB/SIMULINK environment [14].

3.1 Passive harmonic filters

The considered passive harmonic filter (PHF) topologies were investigated in the simulated power system presented in in Figure 3.1(a).

The filters are tuned to the frequency a bit smaller than the frequency of the first high harmonic characteristic (after the fundamental harmonic) for 6-pulse thyristor rectifier, which is the 5th harmonic (4.85th). For each considered filter topologies, the capacitors resistance is neglected, the reactors resistance is computed basing on the quality factor, the compensating reactive power (fundamental harmonic) is constant: Q_f = -2172.5 Var (except in the case of single-tuned topology) as well as the rectifier firing angle. The voltage and current data and characteristics at the thyristor bridge AC side are considered at the steady state.
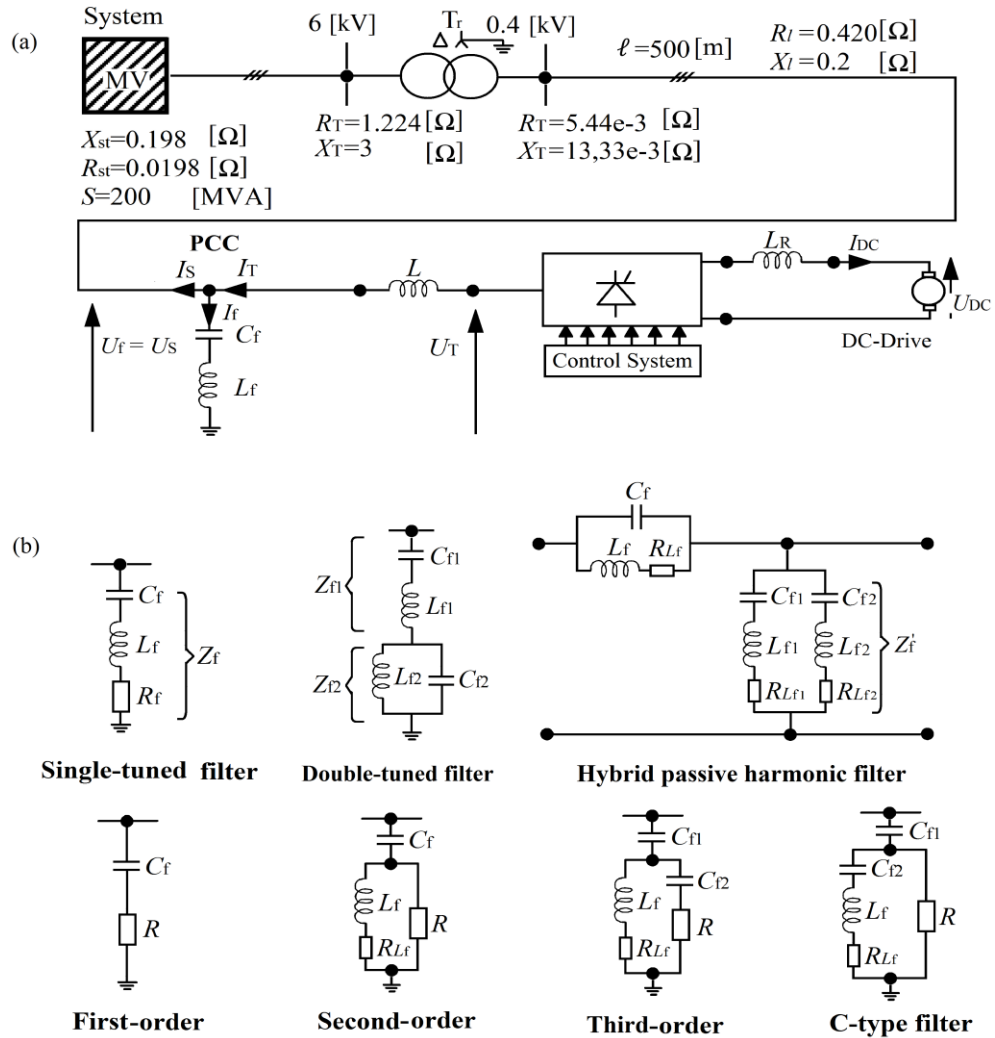
Figure 3.1   (a) Simulated power system, (b) investigated passive parallel harmonic filter topologies

3.1.1 Example of investigatigation performed on the PHF topologies

In this chapter, the single-tuned filter (see Figure 3.1(b)) is studied by presenting the influence of detuning phenomenon on its work efficiency. The formulas used to compute its parameters are presented in Table 3.1.

The single-tuned filter (as other filter topologies) is investigated in frequency domain through its impedance versus frequency versus and in time domain after its connection in the power system in Figure 3.1(a).

Table 3.1   Computation formulas of the single-tuned filter parameters

$$\underline{Z}_\mathrm{f}(j\omega) = R_\mathrm{f} + j\omega L_\mathrm{f} - j\frac{1}{\omega C_\mathrm{f}}$$

$$\underline{Z}_\mathrm{f}(j\omega_{(n)}) = R_\mathrm{f} + j\left(n\omega_{(1)}L_\mathrm{f} - \frac{1}{n\omega_{(1)}C_\mathrm{f}}\right)$$

$$\omega_{(n)} = n\omega_{(1)}, \quad R_\mathrm{f} = \frac{1}{q''}\sqrt{\frac{L_\mathrm{f}}{C_\mathrm{f}}}$$

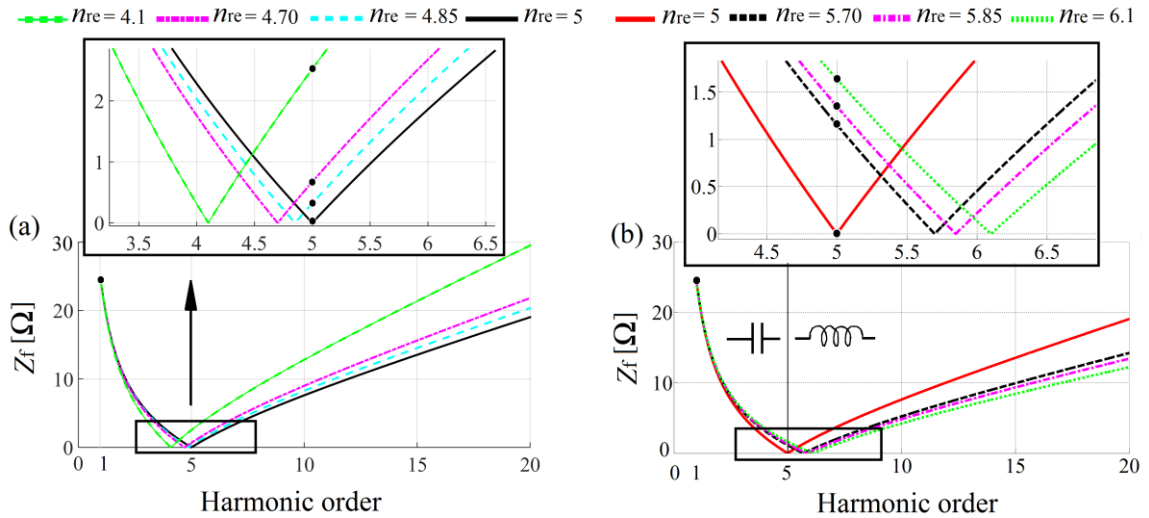| $R_\mathrm{f} = 0$	
$\underline{Z}_\mathrm{f}(j\omega_\mathrm{re}) \rightarrow 0 \Rightarrow j\dfrac{\omega_\mathrm{re}^2 L_\mathrm{f} C_\mathrm{f} - 1}{\omega_\mathrm{re} C_\mathrm{f}} = 0 \Rightarrow \omega_\mathrm{re} = \dfrac{1}{\sqrt{L_\mathrm{f}C_\mathrm{f}}}$ $= n_\mathrm{re}\omega_{(1)}$	$\underline{Z}_\mathrm{f}(j\omega_{(1)}) = j\dfrac{\omega_{(1)}^2 - \omega_\mathrm{re}^2}{\omega_\mathrm{re}^2 \omega_{(1)} C_\mathrm{f}} = j\dfrac{1 - n_\mathrm{re}^2}{n_\mathrm{re}^2 \omega_{(1)} C_\mathrm{f}}$
$Q_\mathrm{f} = U_\mathrm{f}I_\mathrm{f} = \dfrac{U_\mathrm{f}^2}{Z_\mathrm{f}}$	$C_\mathrm{f} = \dfrac{n_\mathrm{re}^2-1}{n_\mathrm{re}^2}\dfrac{Q_\mathrm{f}}{\omega_{(1)}U_\mathrm{f}^2}, \; n_\mathrm{re}^2 > 1$
$L_\mathrm{f} = \dfrac{1}{C_\mathrm{f}\omega_{(1)}^2 n_\mathrm{re}^2} = \dfrac{1}{n_\mathrm{re}^2 - 1}\dfrac{U_\mathrm{f}^2}{\omega_{(1)}Q_\mathrm{f}}$	$X_\mathrm{Cf} = \dfrac{n_\mathrm{re}^2}{n_\mathrm{re}^2 - 1}\dfrac{U_\mathrm{f}^2}{Q_\mathrm{f}}, X_\mathrm{Lf} = \dfrac{1}{n_\mathrm{re}^2 - 1}\dfrac{U_\mathrm{f}^2}{Q_\mathrm{f}}$
$X_\mathrm{re} = \sqrt{\dfrac{L_\mathrm{f}}{C_\mathrm{f}}}$	$U_\mathrm{Cf} = \dfrac{n_\mathrm{re}^2}{n_\mathrm{re}^2 - 1}U_\mathrm{f}$

Figure 3.2   Impedance frequency characteristics of single-tuned filter for different values of tuning frequency order. The filter is tuned to the harmonic frequencies lower (a) and higher (b) than the frequency of 5$^\text{th}$ harmonic ($R_\mathrm{f} = 0$)

Because of the aging (it concerns more the capacitor [5]) or work conditions etc., the single filter must be tuned to the frequency a bit smaller than the frequency of lowest generated harmonic (ω_re); in the considered example, the 5$^\text{th}$ order. There are different opinions on how much it should be detuned [4]. According to [10] the detuning frequency should be in the range of 3 to 15% below the frequency of harmonic to be eliminated. In this chapter, the detuning frequencies are chosen between 1% to 20% below the frequency of 5$^\text{th}$ harmonic.

For the tuning frequencies lower (Figure 3.2(a)) or higher (Figure 3.2(b)) than $\omega_{re(5)}$, the filter impedance of the 5th harmnic is high which reduces the filter filtration efficiency. In the case when the filter is detuned to the frequencies higher than $\omega_{re(5)}$, the amplification of the filtered harmonic (5th) can occur because of the parallel resosnamce phenomenon between the filter and the grid inductance.

The equivalent impedance of the filter is capacitive for all harmonics frequencies (also fundamental) lower than the resonance frequency and inductive for the harmonics higher than the resonance component (5th order in Figure 3.2(a) and (b)).

The waveforms of current and voltage at the PCC (Figure 3.1(a)) and their spectrums are presented in Figure 3.3. After the filter connection, it can be observed a little decrease of commutation notches depth (Figure 3.3(a)). The grid current waveforms before and after the filter connection is shown in Figure 3.3(c).

With the decrease of tuning frequency (5th to 4.1st), the amplitude of 5th harmonic of PCC voltage and current (Figure 3.3(b) and (d)) has increased as well as the amplitude of higher harmonics (11th to 29th). The THD of PCC current and voltage has also increased.

The grid voltage and current fundamental harmonic amplitudes are almost constant during the change of the tuning frequency (Figure 3.3(b) and (d)). Nevertheless, after the filter connection, the current has considerably decreased (from 15.86 A to 8.43 A) because of the reactive component compensation.

The filter current spectrum is presented in Figure 3.4(b) and the waveform in Figure 3.4(a). The quantity of filtered harmonic (5th) flowing through the filter depends upon the tuning frequency. Its value is high for the tuning frequency near to the frequency of the 5th harmonic (250 Hz). The single-tuned filter is much loaded by the filtered harmonic than the other harmonics (Figure 3.4(b)).

The single-tuned filter effectiveness is presented in Figure 3.4(c) and (d). The filter is more effective when it is tuned to the frequency smaller but near to the frequency of the filtered harmonic.
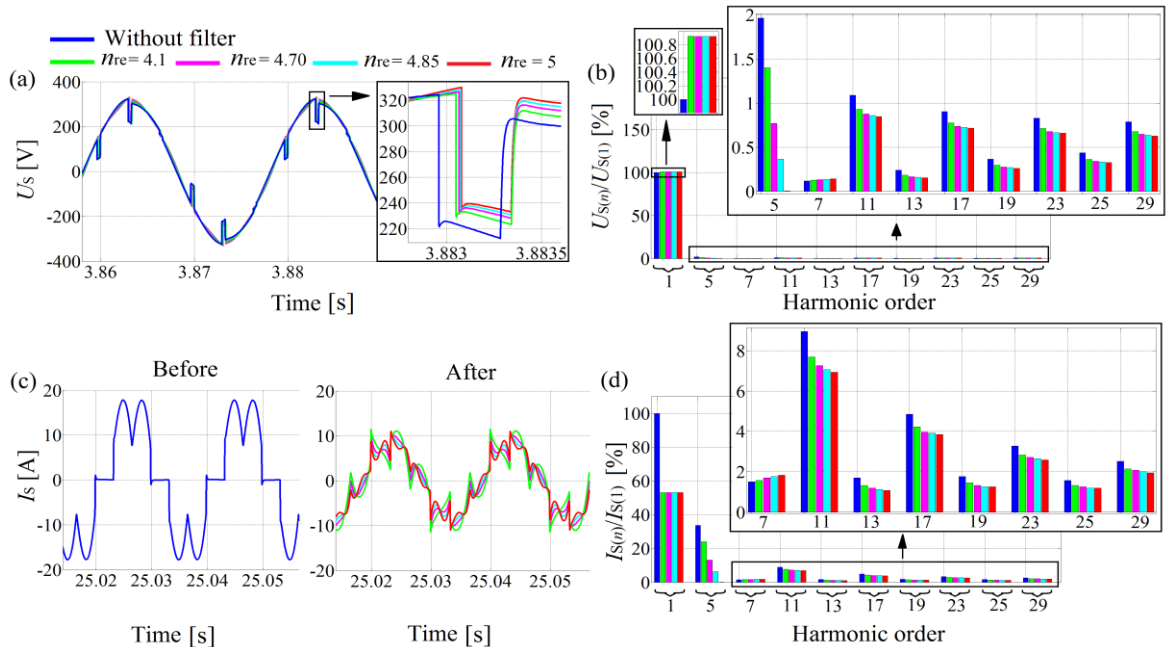

Figure 3.3   (a) grid voltage wavefoms with its spectrum (b), (c) grid current wavefoms with (d) its spectrum
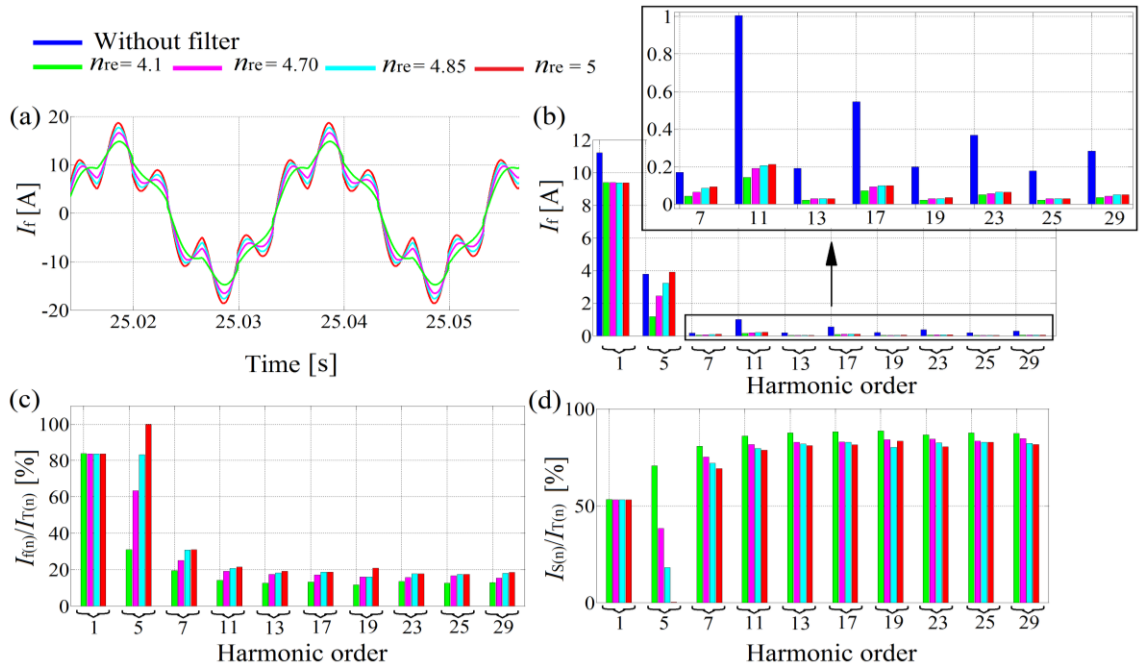
Figure 3.4   (a) filter current waveforms and (b) its spectrum; (c), (d) filter effectiveness
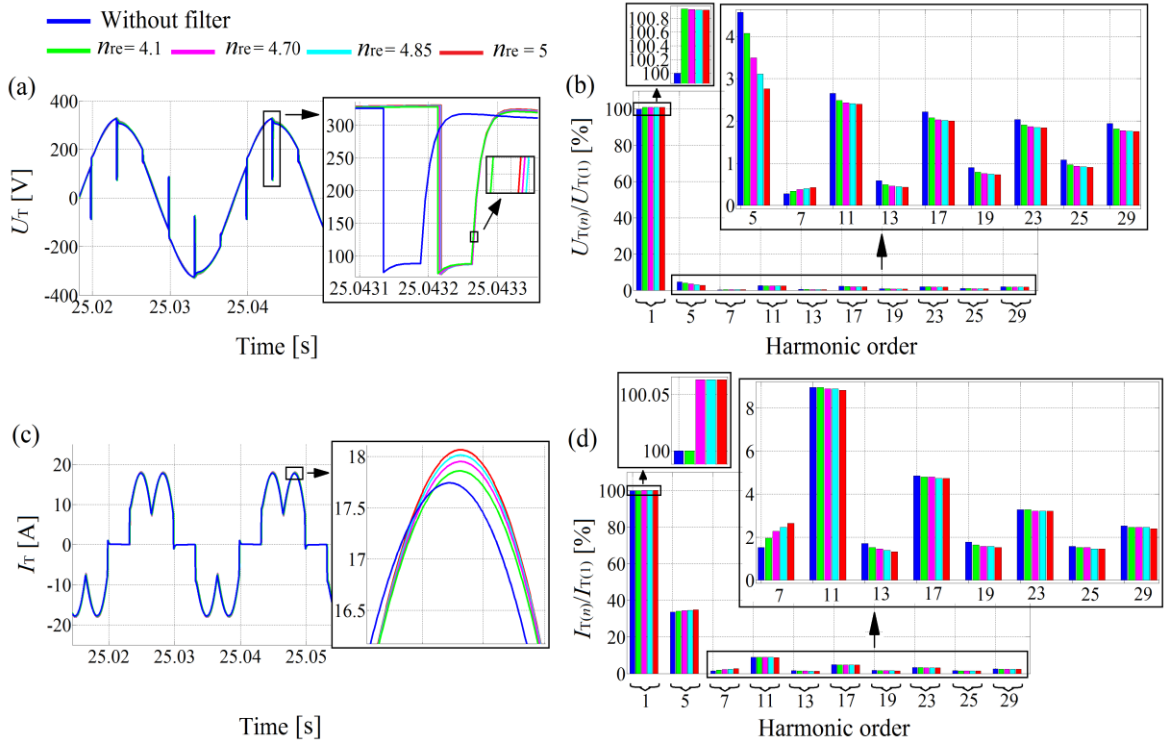

Figure 3.5   (a) voltage at the input of rectifier and (b) its spectrum, (c) current at the input of rectifier (d) its spectrum

The waveforms of voltage and current at the input of thyristor bridge and their spectrums are presented in Figure 3.5.

The power system impedance versus frequency measured from the input terminals of thyristor bridge is presented in Figure 3.6. On the zoom of that figure, the top of the characteristics represents higher impedance value (parallel resonance), and the bottom represents lower impedance value (series resonance). With the decrease of tuning frequency, the displacement of parallel and series resonances from the higher to lower frequency can be observed. The amplitude of power system impedance at the parallel resonance has decreased.
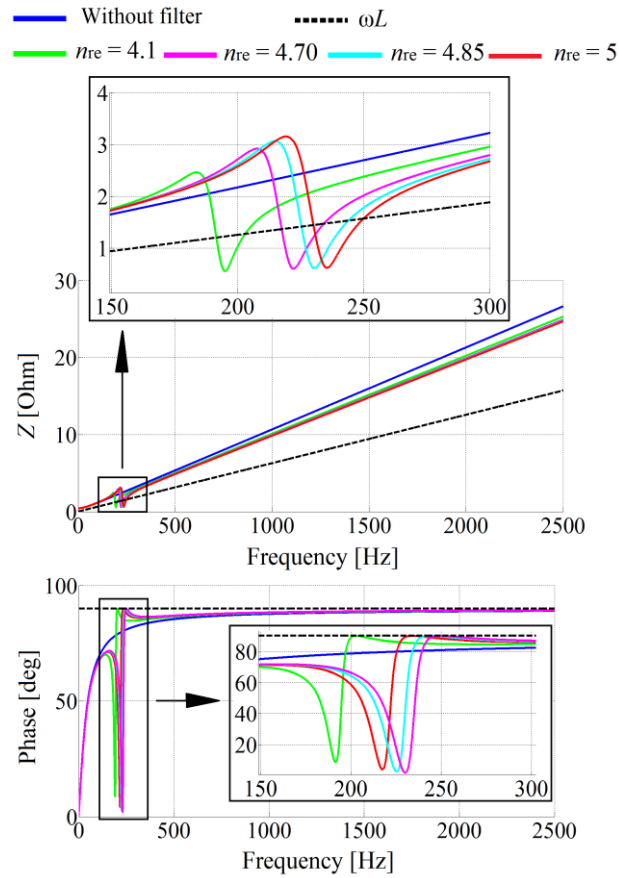
Figure 3.6   Characteristics of power system impedance versus frequency (module and phase) at the thyristor bridge input, ωL- input rectifier reactor reactance
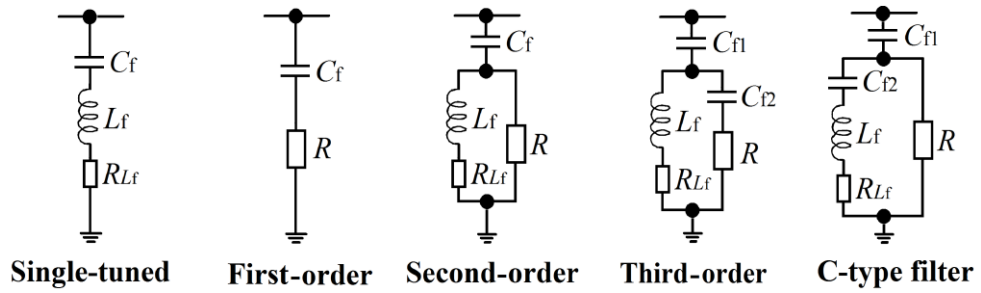
3.1.2   Comparison between the PHF structures

Figure 3.7   Compared topologies

Table 3.2   comparison assumptions

	Qf = -2172.5Var, $\theta = 57°$, $n_{re} = 4.85$, $q' = 85$				
	First-order	Single-tuned	Second-order	third-order	C-type
R [Ω]	-	-	0.08	0.08	0.08
	-	-	1.25	1.25	1.25
	-	-	8	8	8
	-	-	25	25	25
R_{Lf} [Ω]	-	0.0127	0.0127	0.0043	0.0127

After a detail study of PHF topologies, some of them (see Figure 3.7) are compared basing on certain set of criteria: the filter power losses (ΔP_f), the PCC voltage and current 5th harmonic

amplitude ($U_{S(5)}$, $I_{S(5)}$) and the PCC voltage and current THD (THD$_{US}$, THD$_{IS}$). The compared filters are assumed to have the same reactive power ($Q_f = 2172.5$ Var), reactor quality factor ($q' = 85$) and tuning frequency ($n_{re} = 4.85$) (see Table 3.2).

The first-order filter resistance is neglected and the second-order, third-order and C-type filter are assumed to have the same damping resistances (e.g. 0.08 Ω, 1.25 Ω and 25 Ω, see Table 3.2). The single-tuned filter and the first-order filter are compared to the second-order, third-order and C-type filter when the damping resistance of these latest are increasing (from 0.08 Ω to 25 Ω).

All the broad-band filters present the problem of harmonics amplification. But depending on their damping resistance, this problem can be mitigated. From the point of view of individual harmonic mitigation, the single-tuned filter is more recommendable than other topologies because it has the lowest amplitude of grid voltage and current 5th harmonic (Figure 3.8(a)(b)).

With small values of damping resistance (e.g. 0.08 Ω, 1.25 Ω), the third-order filter is more recommendable for the reduction of individual harmonic than the second-order and C-type filter and then come the second-order filter (Figure 3.8(a)(b)).
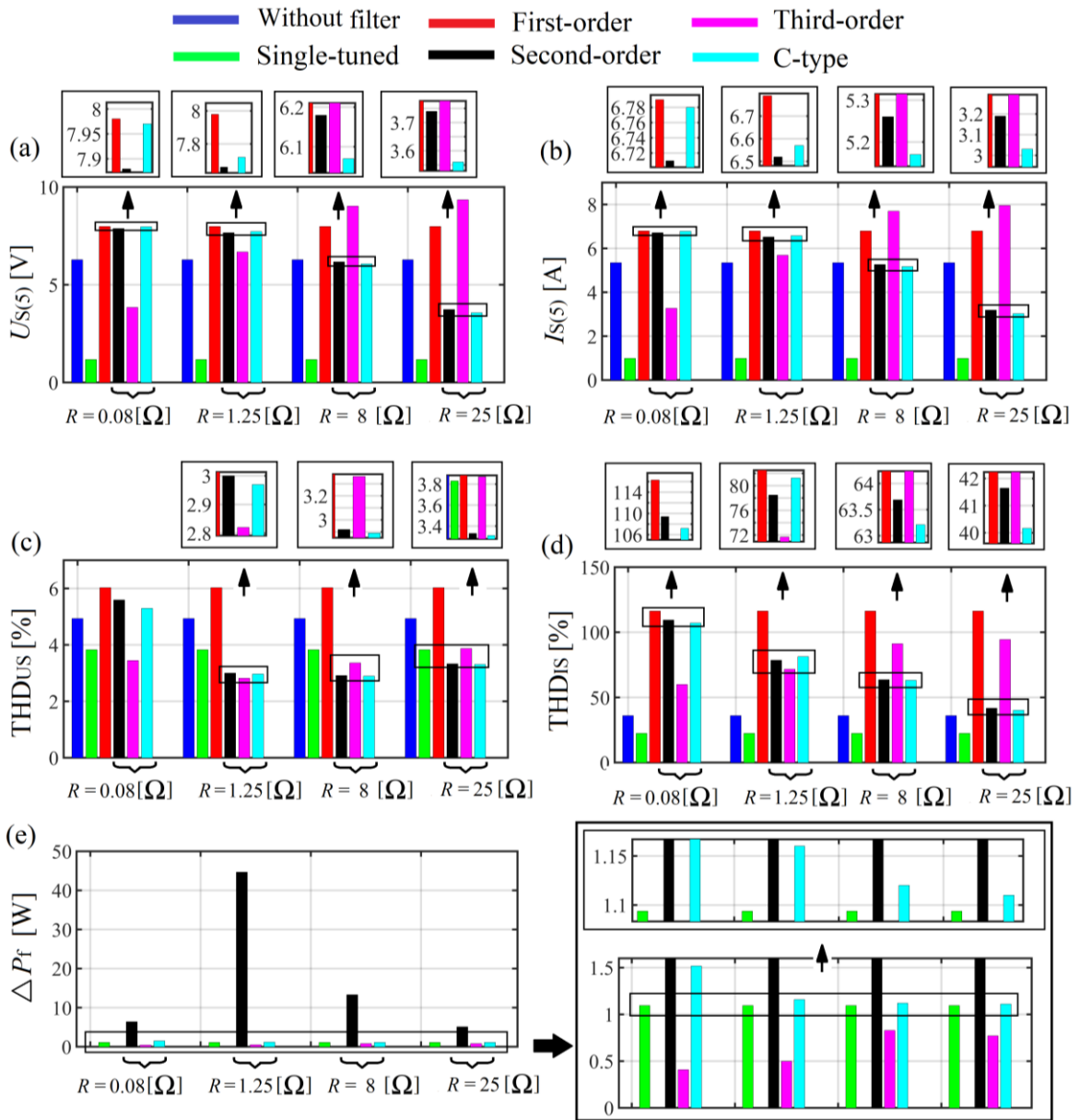

Figure 3.8   Comparison spectrums between the single-tuned, first-order, second-order, third-order filter and C-type filter: (a), (b) grid voltage and current 5th harmonic; (c), (d) grid voltage and current THD; (e) filter power losses

9

With high values of damping resistance (e.g. 8 Ω, 25 Ω), the C-type filter is more recommendable for the reduction of individual harmonic than the second-order and third-order filter. The second-order filter is more recommendable than third-order the filter (Figure 3.8(a)(b)).

From the point of view of the 5th harmonic non-amplification (Figure 3.8(a)(b)), the single-tuned filter is more recommendable, then com the C-type filer with high damping resistance value (e.g. 25 Ω). The third-order filter with high damping resistance value has more probability to amplify the 5th harmonic than other filter.

From the grid voltage distortion point of view, it can be seen in Figure 3.8(c) that the third-order filter is more recommendable than other filters when its damping resistance is small (e.g. 0.08 Ω, 1.25 Ω), and the C-type filter is more recommendable than other filters for high damping resistance (e.g. 8 Ω, 25 Ω) (Figure 3.8(c)).

The single-tuned filter has the lowest PCC current THD than the broad-band filters (Figure 3.8(d)). For small values of R (e.g. 0.08 Ω, 1.25 Ω), the third-order filter is more recommendable than the second-order and C-type filter. For high values of R (e.g. 8 Ω, 25 Ω) it is better to apply the C-type filter than the second-order and third-order filter to improve the grid current THD. The first-order filter has the highest grid current and voltage THD and is not recommendable for harmonics mitigation.

The third-order filter generates less power losses than the single-tuned, second-order and C-type filter (Figure 3.8(e)) and then comes the single-tuned filter and at the end the C-type filter. The second-order filter is the one with the highest power losses.

Comparing the second-order filter to the C-type filter, it can be noticed in (Figure 3.8(a)(b)(c)(d) that, they have almost the same characteristics but from the power losses point of view, the C-type filter is more recommendable.

In the filter group where the basic harmonics such as the 5th, the 7th etc. (from e.g. the adjustable speed drive load) are reduced by the single-tuned filters, the damping filters such as the second-order, third-order or C-type filter can be added for better mitigation of high harmonics in wide band.

The knowledge of PHFs exists for many decades. Although it appears to be very rich, as indicates the experience of the authors. Still in the design process, often too little attention is paid on the analysis of changes filtration properties of these systems [8]. They vary due to many factors, including e.g. aging or manufacturing tolerances of the reactors and capacitors during the manufacturing process etc. [6, 12, 13]. The aim of this chapter was to present the various topologies properties of PHFs using the impedance frequency characteristics [1, 3, 9, 11].

3.1.3 Investigation on the methods of sharing the total reactive power in the filter group

In the PHF domain, there are other problems that needed to investigated. For instance, the parallel connected PHF structures working in-group with a given total reactive power. The question that the engeneer shoul solved is how to share the total reactive power in the filter group? there are different method but in this chapter, six of them are investigated (Table 3.3).

To determine which method (A-F) is the best, a set of criteria has been established in Table 3.4. Observing that table, it can be noticed different filtration efficiency and in general sense it is difficult to indicate which method is the most effective because there is not big difference between the compared parameters.

Table 3.3　　　Expressions used to compute the reactive power of each filter in the group for each method
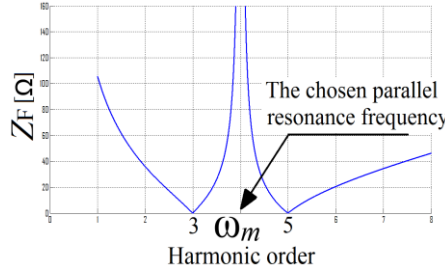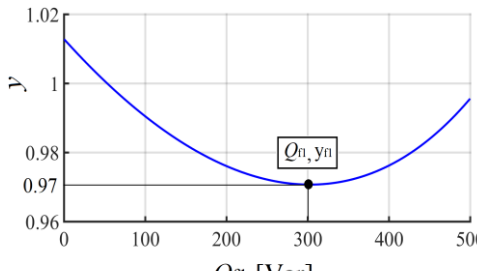
Method A - equal reactive power for filters	$Q_{f1} = Q_{f2} = \dfrac{Q_F}{2}$
Method B - the reactive power of filters is inversely proportional to the harmonic order	$\dfrac{Q_{f1}}{Q_{f2}} = \dfrac{n_{re\_f2}}{n_{re\_f1}} \Rightarrow 2.9Q_{f1} = 4.85Q_{f2} \Rightarrow Q_{f1} = \dfrac{2.9}{7.75}Q_F$
Method C - the reactive power of filters is inversely proportional to the square of harmonic order	$\dfrac{Q_{f1}}{Q_{f2}} = \dfrac{n_{re\_f2}^2}{n_{re\_f1}^2} \Rightarrow 8.41Q_{f1} = 23.52Q_{f2} \Rightarrow Q_{f1}$ $= \dfrac{8.41}{31.93}Q_F$
Method D - the reactive power of filters is calculated on the base of the shaping of frequency characteristic of the filter impedance	The chosen parallel resonance frequency Harmonic order $\left\{ \begin{bmatrix} \dfrac{2.9^2 * 100\pi}{1 - 2.9^2} & \dfrac{4.85^2 * 100\pi}{1 - 4.85^2} \\ \dfrac{2.9^2 * 4}{4^2 - 2.9^2} & \dfrac{4.8^2 * 4}{4^2 - 2.9^2} \end{bmatrix} \begin{bmatrix} C_{f1} \\ C_{f2} \end{bmatrix} = \begin{bmatrix} \dfrac{Q_F}{230^2} \\ 0 \\ 0 \end{bmatrix} \right.$
Method E - the reactive power of filters is calculated on the base of the assumption that the reactors of filters are identical	$Q_{f1} = \dfrac{Q_F}{(1-2.9^2)\left(\dfrac{1}{1-2.9^2}+\dfrac{1}{1-4.85^2}\right)}$
Method F (optimization) - $y = 1 - (1 - \varphi_1)(1 - \varphi_2)$	Q_{f1} [Var]

Table 3.4　　　Comparison of the methods basing on the selected criterions

Comparison criteria	Method A	Method B	Method C	Method D	Method E	Method F
$U_{S(3)}$ [v]	0.43	0.41	0.40	0.40	0.40	0.41
$U_{S(5)}$ [v]	0.45	0.48	0.51	0.50	0.52	0.47
$(I_{F(3)}/I_{r(3)})$ [%]	11.16	15	16.66	16.66	16.66	13.33
$(I_{F(5)}/I_{r(5)})$ [%]	31.48	24.07	18.51	22.22	18.51	25.92
THD$_{Us}$[%]	0.50	0.50	0.51	0.51	0.51	0.51
ΔP_F [w]	0.533	0.600	0.660	0.6418	0.6687	0.5897
The blue area indicates which method is the best in comparison to other methods.						

3.2   Shunt active power filter

The investigated shunt active power filter (SAPF) structure is presented in Figure 3.9. During the inveatigations, the author has proposed its own control system alfgorithm based on instantaneous *p-q* theory (see Figure 3.10). The investigations were foccussed on the influence of the electrical grid inductance (grid short-circuit power), the inverter input reactor, DC capacitor and the load input reactor parameters on the SAPF work efficiency.
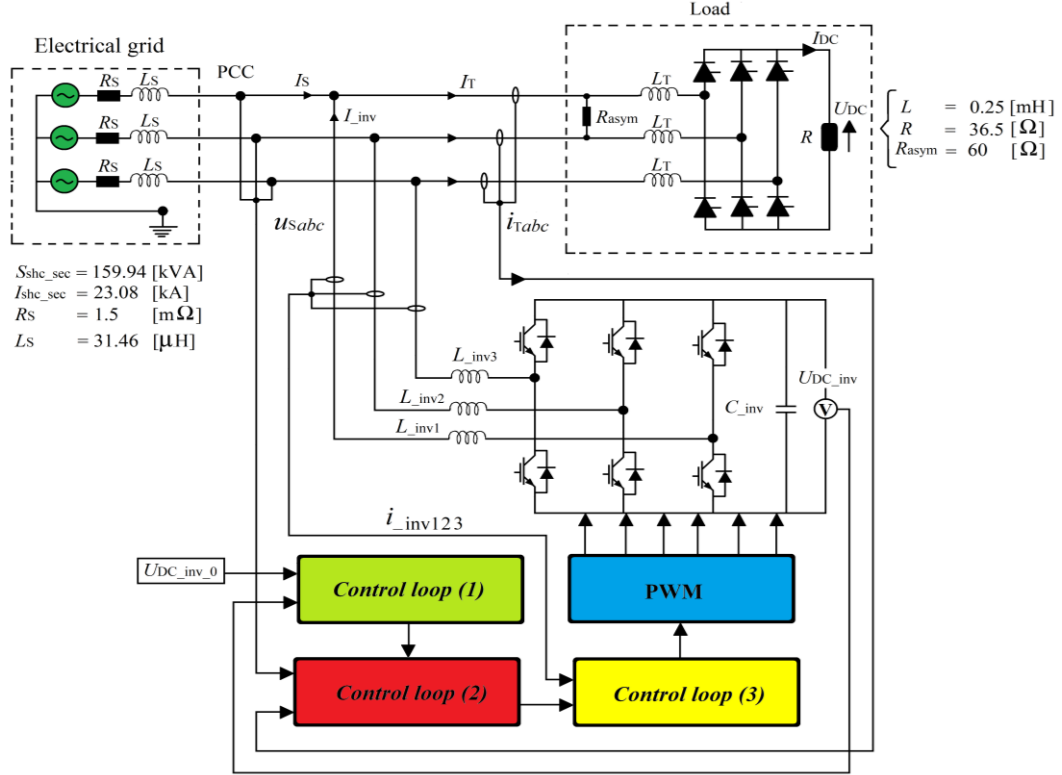

Figure 3.9   Power system together with the SAPF

3.2.1   Example of investigation performed on the SAPF

The investigation on the influence of the thyristor bridge input reactor (L_T) on the SAPF performances is presented in this chapter. The PCC voltage and current waveforms together with spectrums before the SAPF connetion are presented in Figure 3.11.

The grid voltage and current waveforms of Figure 3.12(a)(b)(c) shows that with the thyristor bridge input reactor inductance equal or higher than the inductance at the SAPF input reactor, the ripples (at the points of commutation notches) are reduced (see Figure 3.12(b)(c)).

The fundamental harmonic parameters of grid voltage and current are presented in Table 3.5. With the input rectifier reactor inductance increase, the grid current has little decreased.
The waveform of the reference current compared to the one of the compensating current is presented in Figure 3.13(a)(b)(c). Increasing the rectifier input reactor inductance (L_T) to the value equal or higher than L_{inv_min} has reduced the rectifier input current rate of change at the points of commutation notches making possible the compensating current to track the reference current (Figure 3.13(b)(c)). The error at the PI controller input are presented in Figure 3.14(a)(b)(c) and the waveforms of inverter DC capacitor voltage are considered Figure 3.14(d).
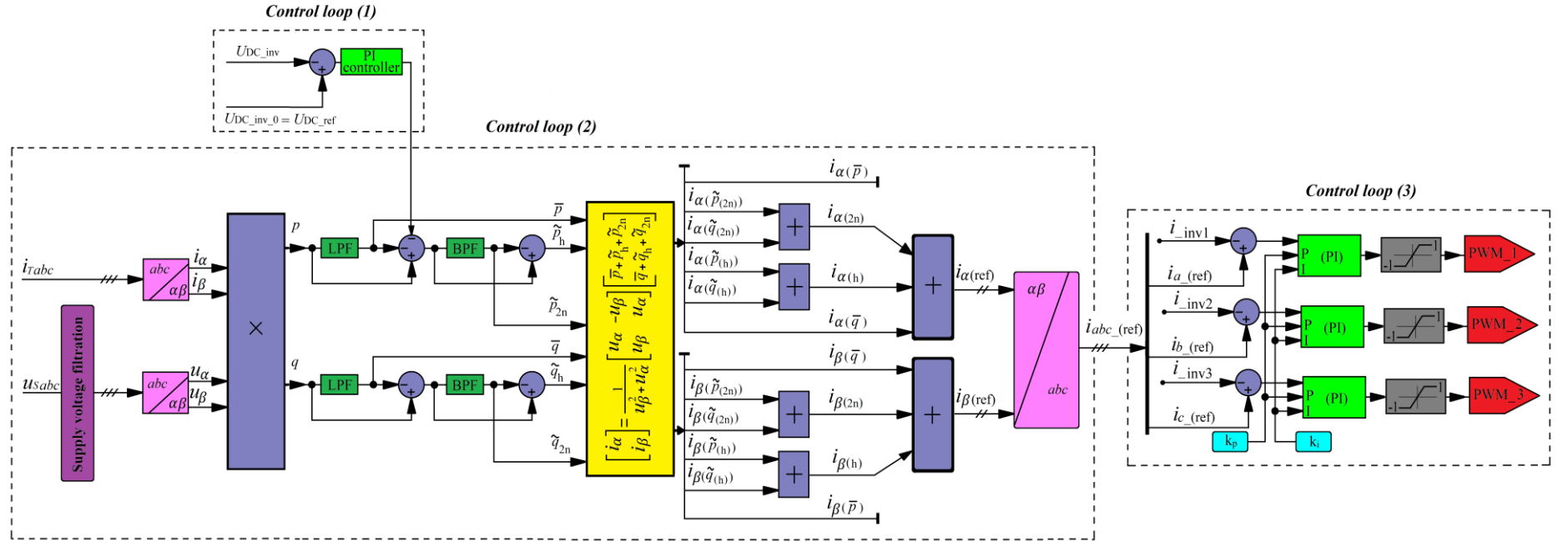
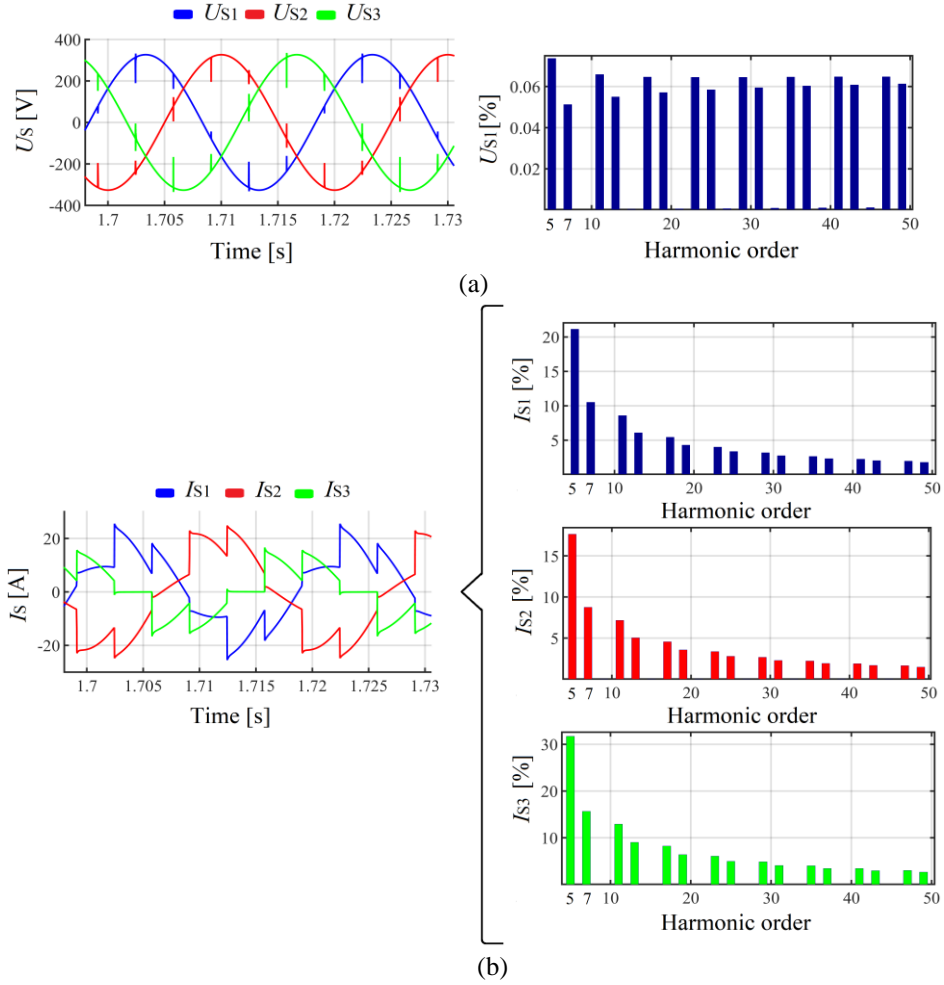Figure 3.10　Proposed SAPF control system

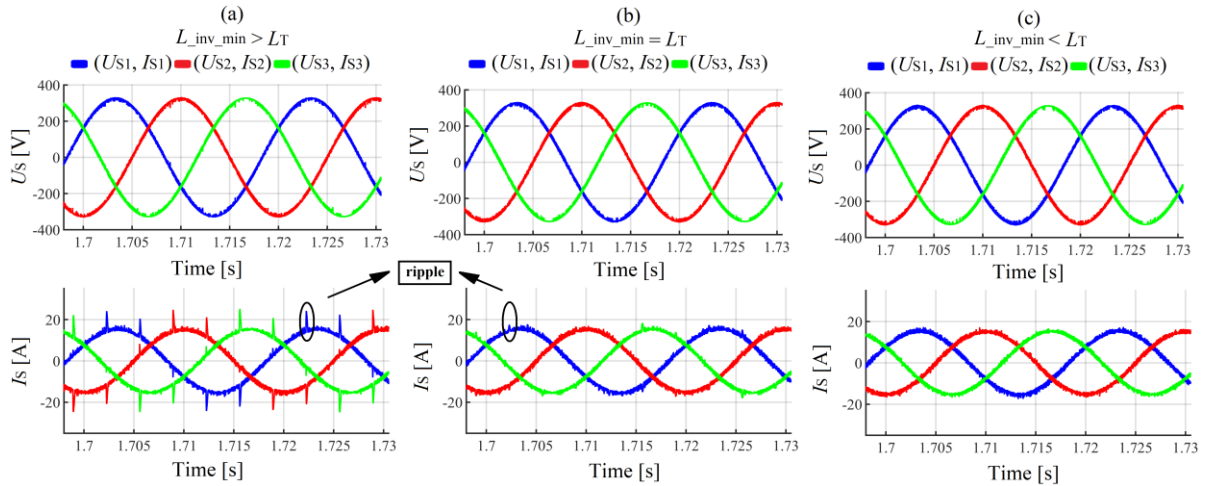Figure 3.11   Waveforms of PCC voltage (a) and current (b) with their spectrums before the SAPF connection

Figure 3.12   Waveforms of PCC voltage and current for different value of input rectifier reactor inductance: (a) $L_{\text{inv\_min}} > L_T$, (b) $L_{\text{inv\_min}} = L_T$, (c) $L_{\text{inv\_min}} < L_T$

Table 3.6 shows that the best results in term of grid current and voltage THD (as well as TTHD – see Table 3.7); fundamental harmonic reactive power compensation and asymmetry compensation are when the $L_{\text{inv\_min}}$ is equal or smaller than L_T.

Table 3.5 Grid voltage and current fundamental harmonic before and after the SAPF connection (for different input rectifier reactor value)

	(Before the SAPF connection) $L_T = 1$ nH				(After the SAPF connection) $L_{\_inv} > L_T$			
	$U_{S(1)}$ [V]		$I_{S(1)}$ [A]		$U_{S(1)}$ [V]		$I_{S(1)}$ [A]	
	RMS	Phase	RMS	Phase	RMS	Phase	RMS	Phase
L1	230.8	30º	12.43	21.7º	230.8	30º	10.41	29.4º
L2	230.7	270º	14.92	235.4º	230.7	270º	10.4	269.2º
L3	230.7	150º	8.29	111.90º	230.7	150º	10.37	149.3º

	(After the SAPF connection) $L_{\_inv\_min} = L_T$				(After the SAPF connection) $L_{\_inv\_min} < L_T$			
	$U_{S(1)}$ [V]		$I_{S(1)}$ [A]		$U_{S(1)}$ [V]		$I_{S(1)}$ [A]	
	RMS	Phase	RMS	Phase	RMS	Phase	RMS	Phase
L1	230.8	30º	10.29	29.4º	230.8	30º	10.14	29.5º
L2	230.7	270º	10.3	269.3º	230.8	270º	10.14	269.3º
L3	230.7	150º	10.28	149.3º	230.8	150º	10.11	149.4º

Table 3.6   Grid voltage and current THD as well as reactive and active power before and after the SAPF connection (for different input rectifier reactor inductance value)

	(Before the SAPF connection) $L_T = 1$ nH					(After the SAPF connection) $L_{\_inv\_min} > L_T$				
	THD$_{US}$ [%]	THD$_{IS}$ [%]	$Q_{S(1)}$ [Var]	$P_{S(1)}$ [W]	k_{asym} [%]	THD$_{US}$ [%]	THD$_{IS}$ [%]	$Q_{S(1)}$ [Var]	$P_{S(1)}$ [W]	k_{asym} [%]
L1	0.25	28.07	414.08	2838.4		0.15	8.77	25.15	2402.5	
L2	0.25	23.41	1954.5	2833.1	33.25	0.15	8.75	33.51	2400.1	0.30
L3	0.25	42.07	1181.8	1507.2		0.15	8.77	29.24	2393.2	

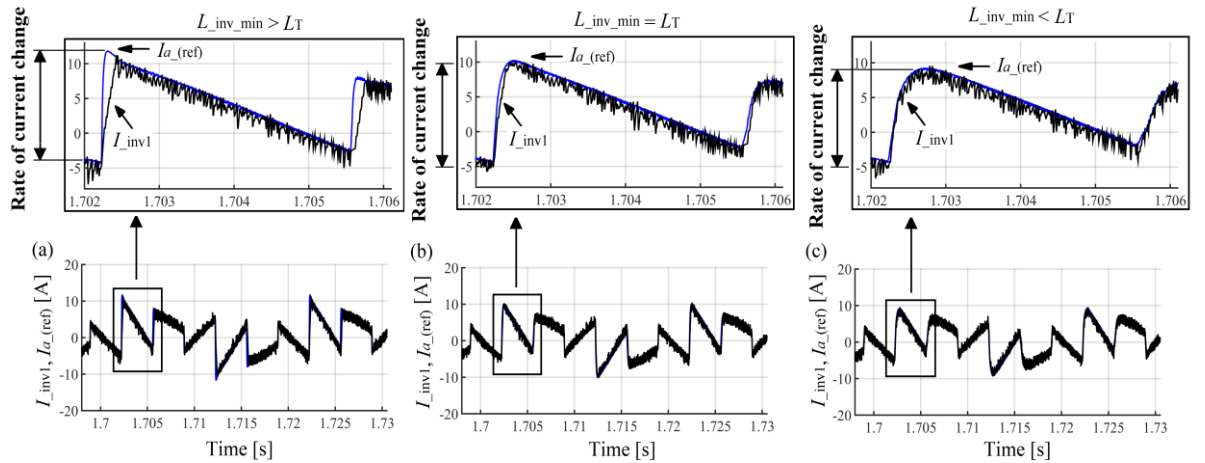|	(After the SAPF connection) $L_{\_inv\_min} = L_T$					(After the SAPF connection) $L_{\_inv\_min} < L_T$				
	THD$_{US}$ [%]	THD$_{IS}$ [%]	$Q_{S(1)}$ [Var]	$P_{S(1)}$ [W]	k_{asym} [%]	THD$_{US}$ [%]	THD$_{IS}$ [%]	Q_{S} [Var]	P_{S} [W]	k_{asym} [%]
L1	0.04	2.47	24.86	2374.8		0.02	1.22	20.42	2340.2	
L2	0.05	2.91	29.04	2377.1	0.30	0.02	1.49	28.59	2340.1	0.20
L3	0.05	2.79	28.98	2372.4		0.02	1.22	24.43	2333.3	

Figure 3.13   Waveforms comparison between the reference and compensating current of *control loop (3)* (Figure 4.24): (a) for $L_{\_inv\_min} > L_T$, (b) for for $L_{\_inv\_min} = L_T$, (c) for $L_{\_inv\_min} = L_T$
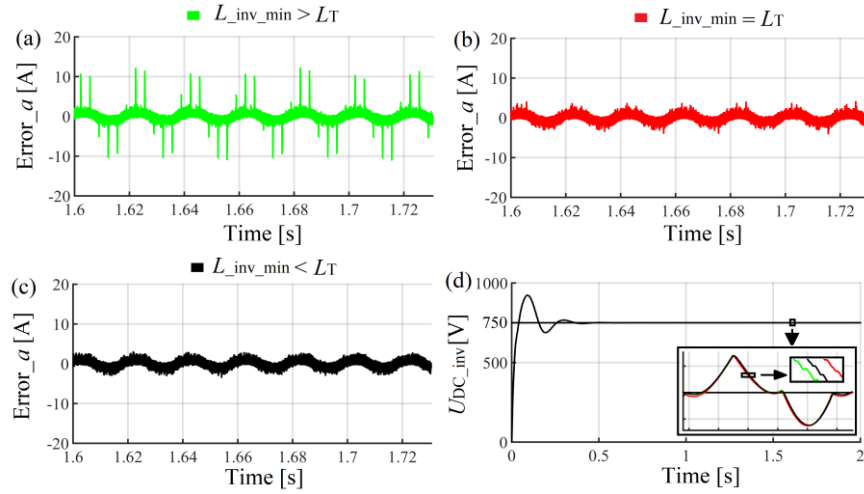
Figure 3.14   (a)(b)(c) error at the input of PI current *control loop (3)*; (d) inverter DC capacitor voltage

Table 3.7   Grid voltage and current TTHD for different value of input rectifier reactor inductance

	(After the SAPF connection) $L_{\_inv\_min} > L_T$		(After the SAPF connection) $L_{\_inv\_min} = L_T$		(After the SAPF connection) $L_{\_inv\_min} < L_T$	
	TTHD$_{US}$ [%]	TTHD$_{IS}$ [%]	TTHD$_{US}$ [%]	TTHD$_{IS}$ [%]	TTHD$_{US}$ [%]	TTHD$_{IS}$ [%]
L1	3.12	12.60	3.18	7.16	3.30	6.59
L2	2.77	13.77	2.85	8.08	2.92	6.82
L3	3.12	13.40	3.23	7.20	3.29	6.11

The performed studies in this chapter allow the author to conclude that the SAPF efficiency did not depend only on its control system and parameters of the elements that constitute it, but also on the electrical grid and load parameters. In the power system with non-sinusoidal voltage and current, the voltage filtration before its use in the algorithm based on instantaneous *p-q* theory is important (from the grid current distortion mitigation point of view).

3.3   Hybrid active power filter

The knowleghes from the investigation on PHF structures and on the SAPF have allowed the author to analyse the hybrid active power filter (HAPF2), structure in which the passive part is connected in series with the passive part as presented in Figure 3.15. The control sytem algorithm presented in Figure 3.18 have been proposed by the author to performed the analysis.

3.3.1   Example of investigation performed on the HAPF2

After connecting the two parts (passive and active), the following question was investigated: to which frequency should be tuend the passive part? Because the thyristor bridge generates characteristic harmonics that are the 5th, 7th, 11th, 13th etc.

To solve that question, three simulation cases studies were investigated and compared: in the first one, the PHF of HAPF2 is tuned to the frequency a little bit lower (e.g. 243.5Hz, 4.87) than the frequency of the first load characteristic harmonic (the 5th). In the second one, it is tuned to the frequency a little bit lower (e.g. 343.5Hz, 6.87) than the frequency of the second load characteristic harmonic (the 7th) and in the third one, it is tuned to the frequency a little bit lower (e.g. 543.5Hz, 10.87) than the frequency of the third load characteristic harmonic (the 11th).

The impedance versus frequency characteristics of the passive part are presented in Figure 3.16 and its parameters are presented in Table 3.8.
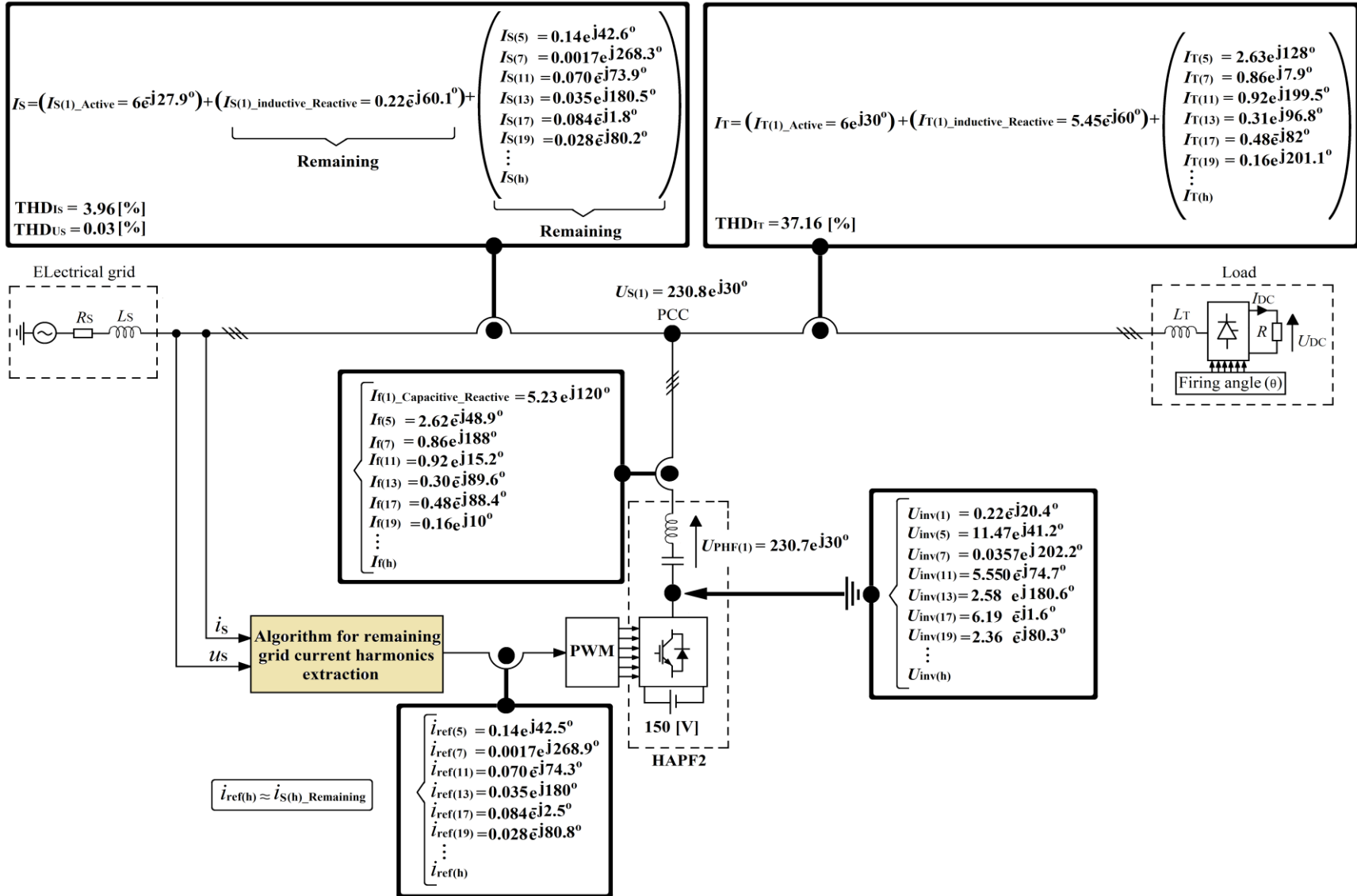
$$I_{S(5)} = 0.14e^{j42.6^o}$$
$$I_{S(7)} = 0.0017e^{j268.3^o}$$
$$I_{S(11)} = 0.070e^{j73.9^o}$$
$$I_{S(13)} = 0.035e^{j180.5^o}$$
$$I_{S(17)} = 0.084e^{j1.8^o}$$
$$I_{S(19)} = 0.028e^{j80.2^o}$$
$$\vdots$$
$$I_{S(h)}$$

$$I_S = \left(I_{S(1)\_Active} = 6e^{j27.9^o}\right) + \left(I_{S(1)\_inductive\_Reactive} = 0.22e^{j60.1^o}\right) +$$

Remaining

Remaining

$$THD_{IS} = 3.96\,[\%]$$
$$THD_{US} = 0.03\,[\%]$$

$$I_{T(5)} = 2.63e^{j128^o}$$
$$I_{T(7)} = 0.86e^{j7.9^o}$$
$$I_{T(11)} = 0.92e^{j199.5^o}$$
$$I_{T(13)} = 0.31e^{j96.8^o}$$
$$I_{T(17)} = 0.48e^{j82^o}$$
$$I_{T(19)} = 0.16e^{j201.1^o}$$
$$\vdots$$
$$I_{T(h)}$$

$$I_T = \left(I_{T(1)\_Active} = 6e^{j30^o}\right) + \left(I_{T(1)\_inductive\_Reactive} = 5.45e^{j60^o}\right) +$$

$$THD_{IT} = 37.16\,[\%]$$

ELectrical grid

R_S L_S

$$U_{S(1)} = 230.8\,e^{j30^o}$$

PCC

Load

L_T I_{DC}

R U_{DC}

Firing angle (θ)

$$I_{f(1)\_Capacitive\_Reactive} = 5.23\,e^{j120^o}$$
$$I_{f(5)} = 2.62e^{j48.9^o}$$
$$I_{f(7)} = 0.86e^{j188^o}$$
$$I_{f(11)} = 0.92\,e^{j15.2^o}$$
$$I_{f(13)} = 0.30e^{j89.6^o}$$
$$I_{f(17)} = 0.48e^{j88.4^o}$$
$$I_{f(19)} = 0.16e^{j10^o}$$
$$\vdots$$
$$I_{f(h)}$$

$$U_{PHF(1)} = 230.7e^{j30^o}$$

$$U_{inv(1)} = 0.22e^{j20.4^o}$$
$$U_{inv(5)} = 11.47e^{j41.2^o}$$
$$U_{inv(7)} = 0.0357e^{j202.2^o}$$
$$U_{inv(11)} = 5.550\,e^{j74.7^o}$$
$$U_{inv(13)} = 2.58\,e^{j180.6^o}$$
$$U_{inv(17)} = 6.19\,e^{j1.6^o}$$
$$U_{inv(19)} = 2.36\,e^{j80.3^o}$$
$$\vdots$$
$$U_{inv(h)}$$

i_S

u_S

Algorithm for remaining grid current harmonics extraction

PWM

150 [V]

HAPF2

$$i_{ref(5)} = 0.14e^{j42.5^o}$$
$$i_{ref(7)} = 0.0017e^{j268.9^o}$$
$$i_{ref(11)} = 0.070\,e^{j74.3^o}$$
$$i_{ref(13)} = 0.035\,e^{j180^o}$$
$$i_{ref(17)} = 0.084e^{j2.5^o}$$
$$i_{ref(19)} = 0.028e^{j80.8^o}$$
$$\vdots$$
$$i_{ref(h)}$$

$$i_{ref(h)} \approx i_{S(h)\_Remaining}$$

Figure 3.15 HAPF2 functionality principle

Table 3.8   HAPF2 passive harmonic filter parameters

n_{re}	L_f [mH]	C_f [μF]	R_{Lf} [mΩ]	Q_f [Var]	q'	L_T [mH]
4.87	6.1	69.74	12.8			
6.87	3.0	71.27	6.3	1210	150	3.5
10.87	1.2	72.19	2.5			
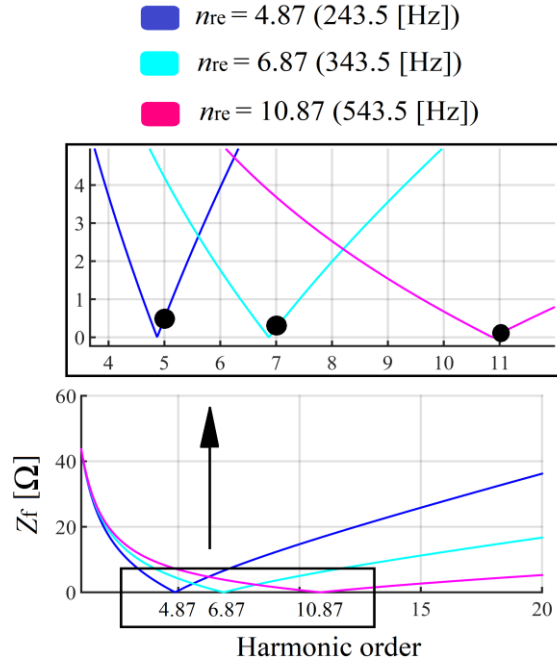
Figure 3.16   PHF impedance versus frequency characteristics. The PHF is tuned to the resonance frequencies of 243.3 Hz, 343.5 Hz and 543 Hz
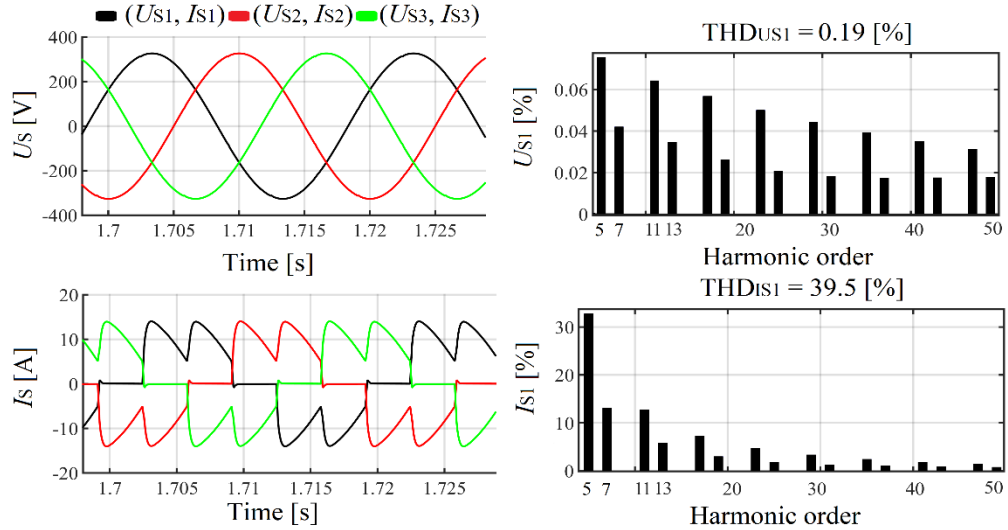

Figure 3.17   Grid voltage (U_S) and current (I_S) waveforms with their spectrums before the HAPF2 connection

The grid voltage and current waveforms with the spectrums before the HAPF2 connection are presented in Figure 3.17. Because of the symmetrical power system, some results are presented only for one-phase. Because of the electrical grid rigidity in the laboratory model (very small inductance in comparison to the rectifier and HAPF2 input inductance), the PCC voltage is very less distorted.
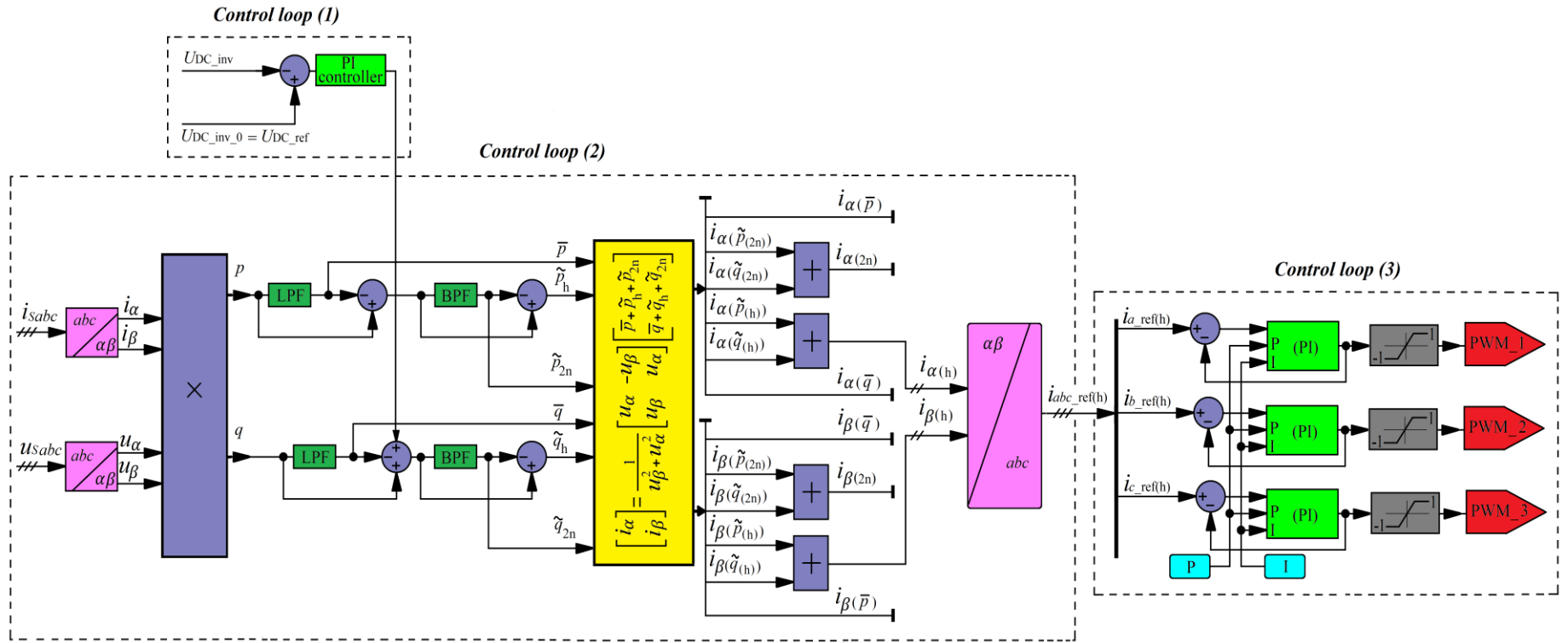
Figure 3.18 HAPF2 control system
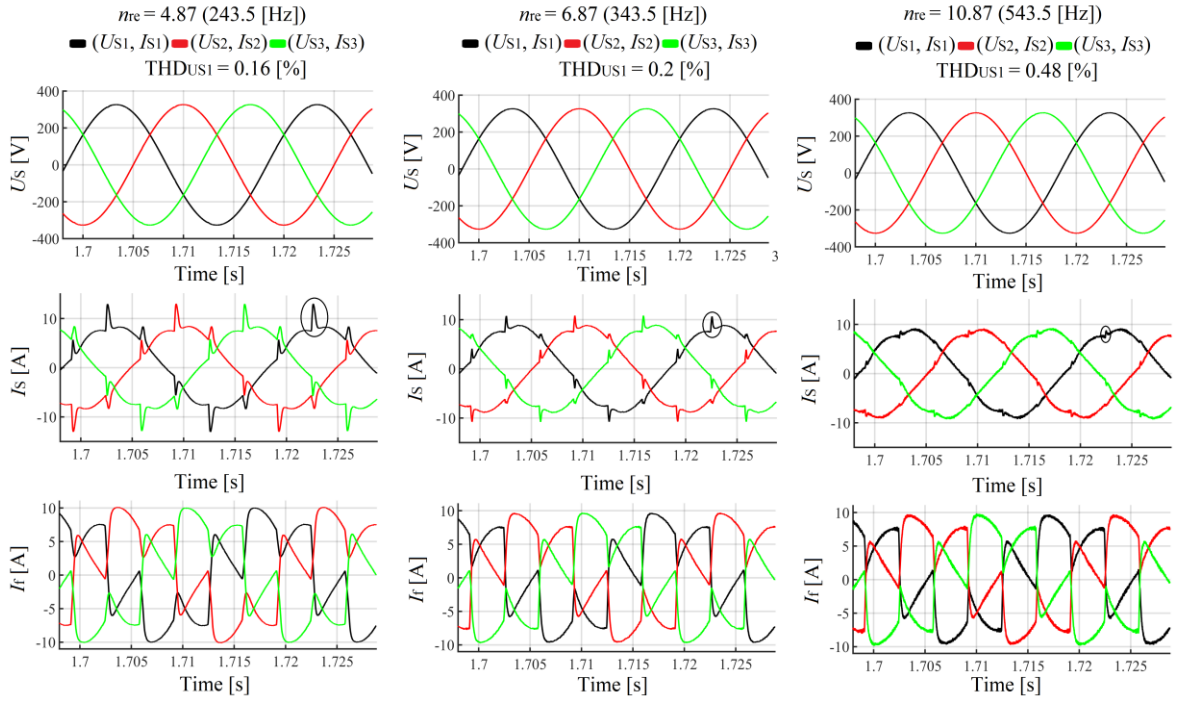
Figure 3.19   Waveforms of grid voltage (Us) and current (Is) and HAPF2 current (I_f) for the PHF tuned to the harmonic component frequency of: 4.87, 6.87 and 10.87
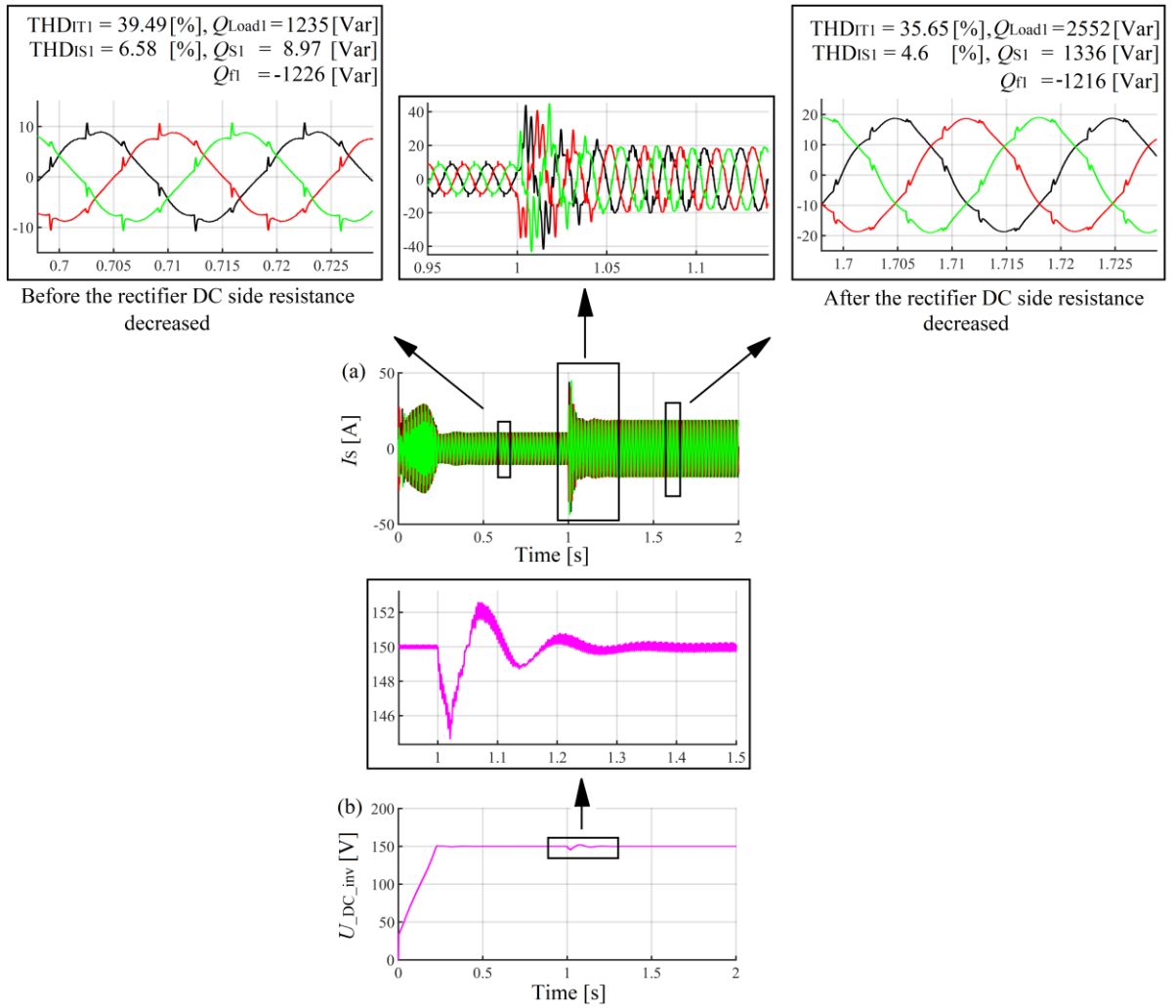
Figure 3.20   (a) grid current waveforms and (b) HAPF2 inverter DC side voltage during the reduction of R_{DC}

In Figure 3.19, the waveforms of grid voltage and current and HAPF2 current after the HAPF2 connection are presented. It can be noticed that the HAPF with PHF tuned to the frequency a little bit lower (e.g. 543.5Hz, 10.87) than the frequency of the 11th harmonic presents the best reduction of the PCC current ripples at the waveforms commutation points. Nevertheless, it presents the highest PCC voltage THD (Figure 3.19).

The simulated power system transient ability during the load parameters change (e.g. decrease of the rectifier DC resistance R_{DC} from 36.5 Ω to 18.25 Ω) is presented in Figure 3.20. It can be seen that after the power system current increase (see Figure 3.20(a) after the rectifier DC side resistance decrease), the HAPF has mitigated the grid current harmonics, but did not totally compensate the fundamental harmonic reactive power because of its PHF reactive power which is sized to around 1210 Var. The invert DC side voltage is shown in Figure 3.20(b).

Figure 3.21(a)(b) presents respectively the waveforms of rectifier input (I_T) and grid side (I_S) current during the asymmetry. The asymmetry was obtained by connecting the resistance beween phases as presented in Figure 3.9 (R_{asym}). The HAPF2 with the proposed control system, does not have ability to compensate the asymmetry component.

The impedance versus frequency observed at the rectifier terminals (Figure 3.22) shows that the power system is purely inductive. The parallel resonance between the PHF (when operating alone) and the electrical gird is completely eliminated as well the dependency of the PHF performances (when operating alone) on the grid impedance.
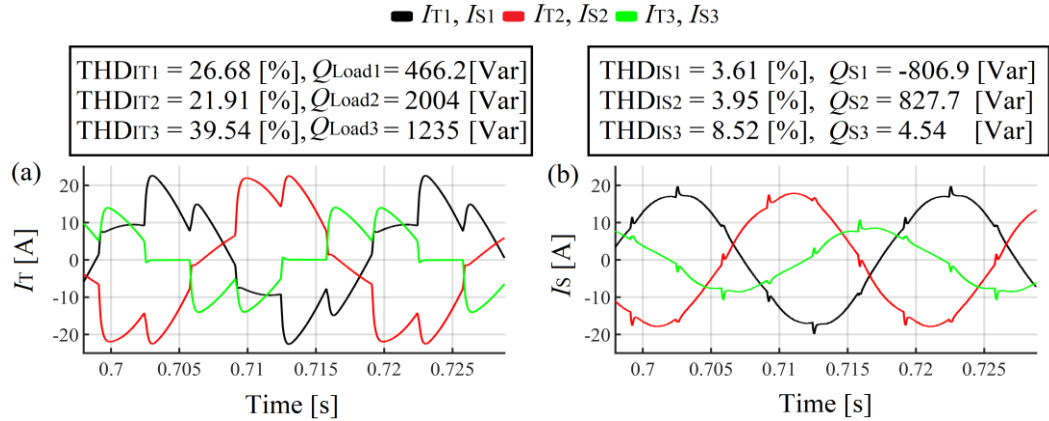
Figure 3.21   Waveforms of (a) input rectifier current and (b) grid current during the load side asymmetry
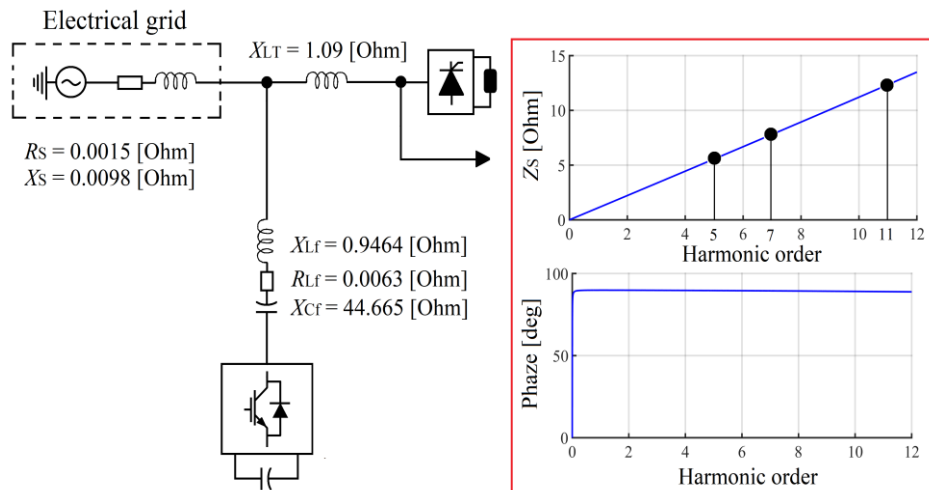

Figure 3.22   Impedance versus frequency of power system observed from thyristor bridge terminals
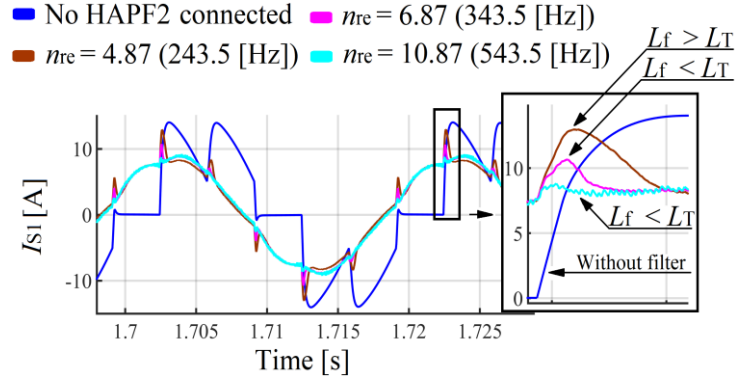
Figure 3.23   Grid current waveforms before and after the HAPF2 connection.

The HAPF2s with passive harmonic filter tuned to the resonance frequency (n_{re} = 6.87 (243.5Hz)) near the frequency of the 7th harmonic and to the resonance frequency (n_{re} = 10.87 (543.5Hz)) near the frequency of the 11th harmonic have the best result in term of grid current THD reduction because the inductances of their reactors which are 3 mH and 1.2 mH respectively are smaller than the input thysristor bridge reactor inductance which is 3.5 mH (see Figure 3.23). Therefore as it has been experimentally demonstrated in chapter 5 that the SAPF input reactor inductance (first-order filter) should be chosen with the value equal or little bit lower than the input rectifier reactor inductance value for a better mitigation of grid current ripple at the waveforms commutation points, that principle should also be applied during the design of HAPF2 passive harmonic filter.

The choose of the HAPF2 passive harmonic filter resonance frequency should not be focused only on the rectifier (load to be compensated) characteristic harmonics but also on the value of the rectifier input reactor inductance. The PHF of HAPF2 can be tuned to any frequency provided that, its reactor inductance has a value equal or smaller than the one of the rectifier input reactor so called commutation reactor.

The performed experiments have also shown that when the PHF is tuned to the resonance frequency higher than the frequencies of the 5th and 7th harmonic: the HAPF reduces (at the grid side) better the higher current harmonics (e.g. from the 13th) because the PHF presents smaller impedance for that harmonics (Figure 3.16.), the 5th and 7th current harmonics are worse reduced and the PHF reactor value is smaller in comparison to the case when it was tuned to the frequency near the 5th or 7th harmonics, therefore low cost. If the PHF reactor value is too small, the HAPF can face the problem of switching ripple mitigation

There are many topologies of PHF that can be connected in series with the SAPF as in the structure of HAPF2 [2].

From this case study of the presented HAPF2 topology, the recommendations can be as following:

− from the grid current perspective, to obtain a lower THD, the passive part tuning frequency should be chosen in the range of higher harmonics, provided that the HAPF input inductance is smaller or equal to the thyristor bridge input inductance,
− from the grid voltage perspective, to obtain a lower THD, the passive part tuning frequency should be chosen in the range of lower harmonics, provided that the HAPF2 input inductance presents better mitigation of the switching ripples harmonics.

4. Laboratory experiments

The electrical grid feeding the laboratory in which the experimental studies were performed, is presented by the equivalent circuit of Figure 4.1(a). The presented examples of laboratory experiments are just to confirm the simulation studies. The electrical network equivalent parameters (impedance, short circuit current and power) are presented in Figure 4.1(b).

The electrical grid voltage (without the considered load) feeding the laboratory is symmetrical (the negative sequence represents 0.12% of the positive sequence) but not pure sinusoidal (Figure 4.2(a)) because of other connected non-linear loads. Its spectrum, limited on one phase as example (Figure 4.2(b)), shows that the dominated harmonics are the 5th (around 2%) and then comes the 3rd (more than 1%) and at the end the 7th (almost 1 %).
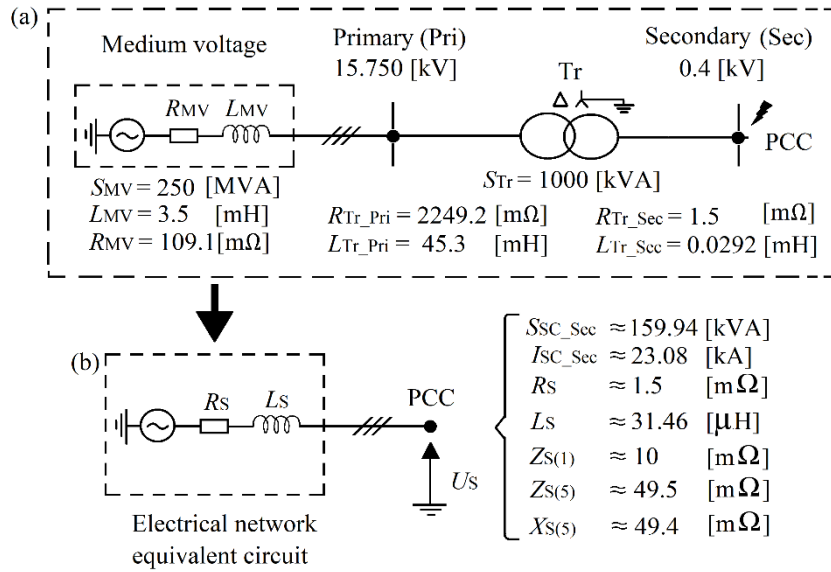
Figure 4.1   (a) laboratory electrical network, (b) electrical grid equivalent circuit
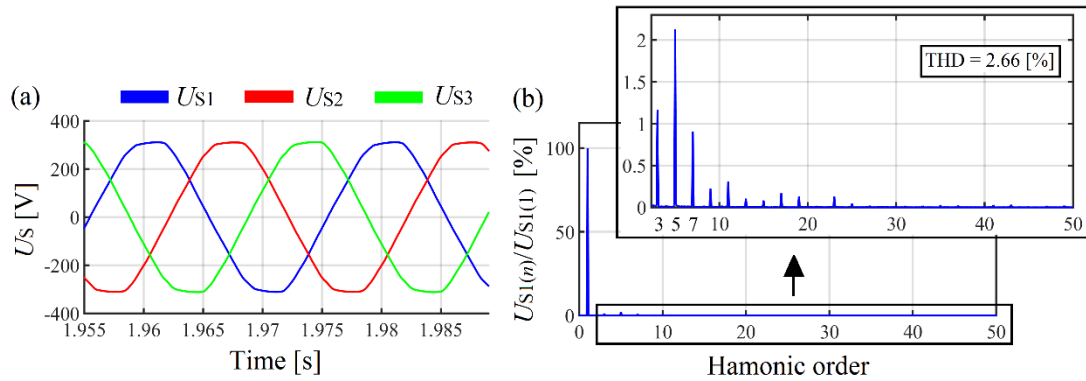
Figure 4.2   (a) PCC voltage waveforms without the considered load connected) and (b) its spectrum (p.u.)

4.1   Passive harmonic filters

The laboratory set up in which the PHFs were investigated is presented in Figure 4.3. The studied PHF topologies are presented in Figure 4.4.

The spectrums in Figure 4.5 present the grid voltage and current harmonics for different values of rectifier firing angle and DC voltage. Owing to the fact that the power system of the designed laboratory model is symmetrical, the results are focussed one one-phase only (see waveforms of Figure 4.5).

Concerning the grid voltage fundamental harmonic, its amplitude has slightly decreased with U_{DC} increase (e.g. from 226.97 V (U_{DC} = 50 V) to 226.13 V (U_{DC} = 525 V)). The 5th harmonic has the highest amplitude for U_{DC} equal to 250 V and the 7th harmonic for U_{DC} to 350V (Figure 4.5).

Apart the 3rd and 9th, there are other non-characteristic harmonics present in the PCC voltage and current spectrums (see Figure 4.6). Looking at the spectrum of Figure 4.6 it is noticed that with the harmonic order increase, some of the non-characteristic harmonics have higher amplitude than the amplitude of characteristic harmonics.
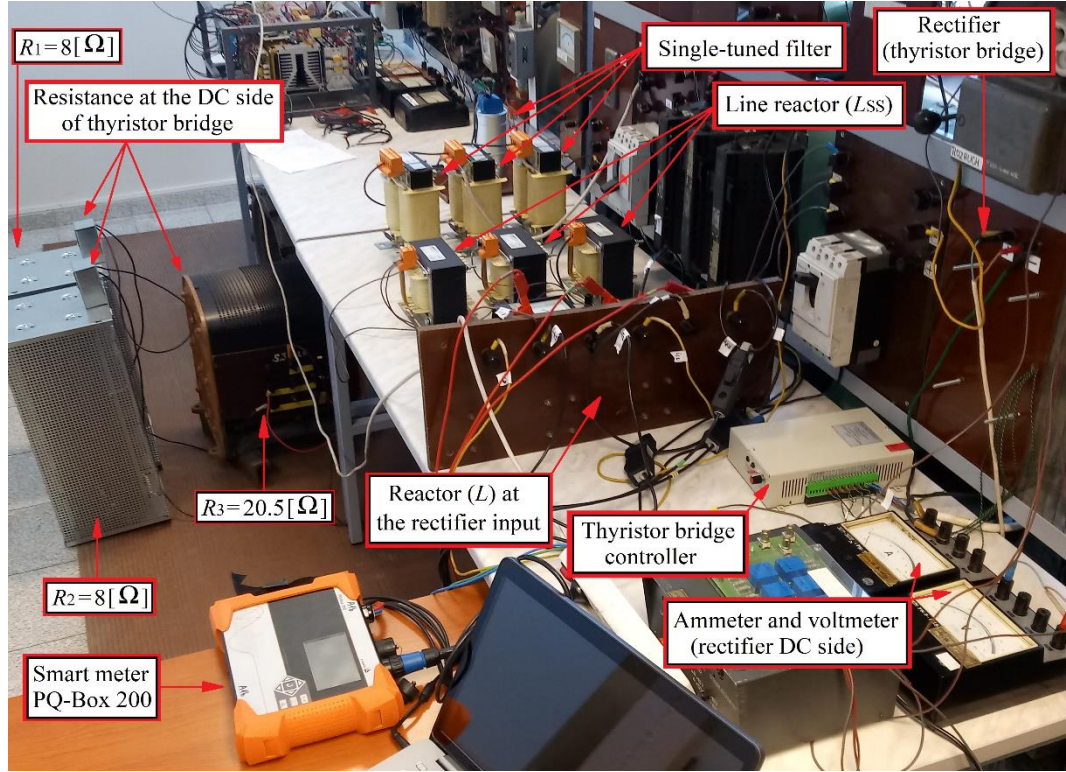
Figure 4.3   Laboratory model
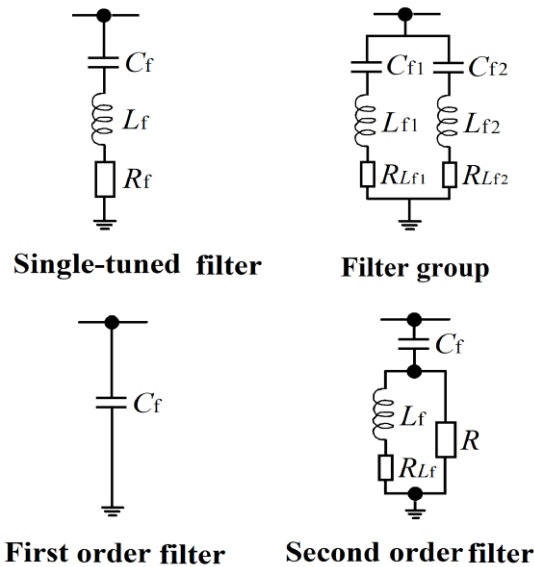
Figure 4.4   Investigated PHF topologies in the laboratory
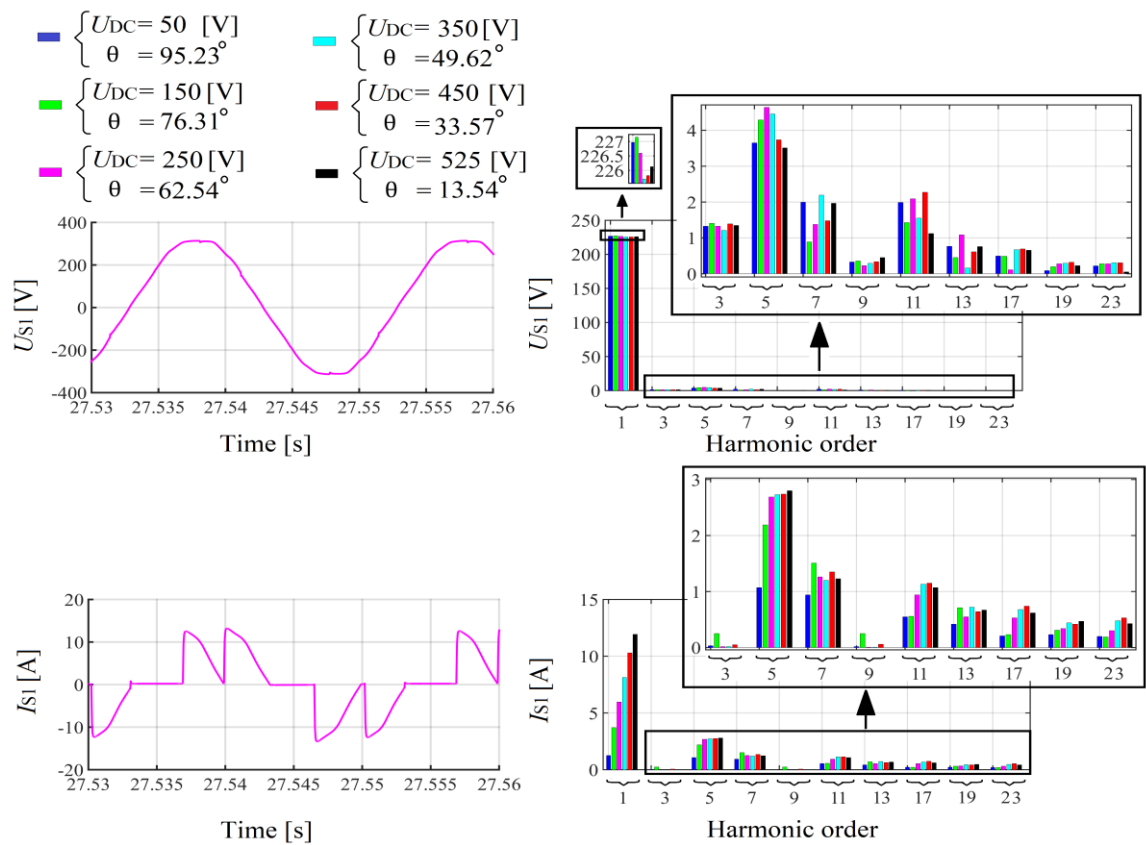
Figure 4.5   Grid voltage and current parameters measured from the laboratory model. The example of waveforms are for the U_{DC} equal to 250 V
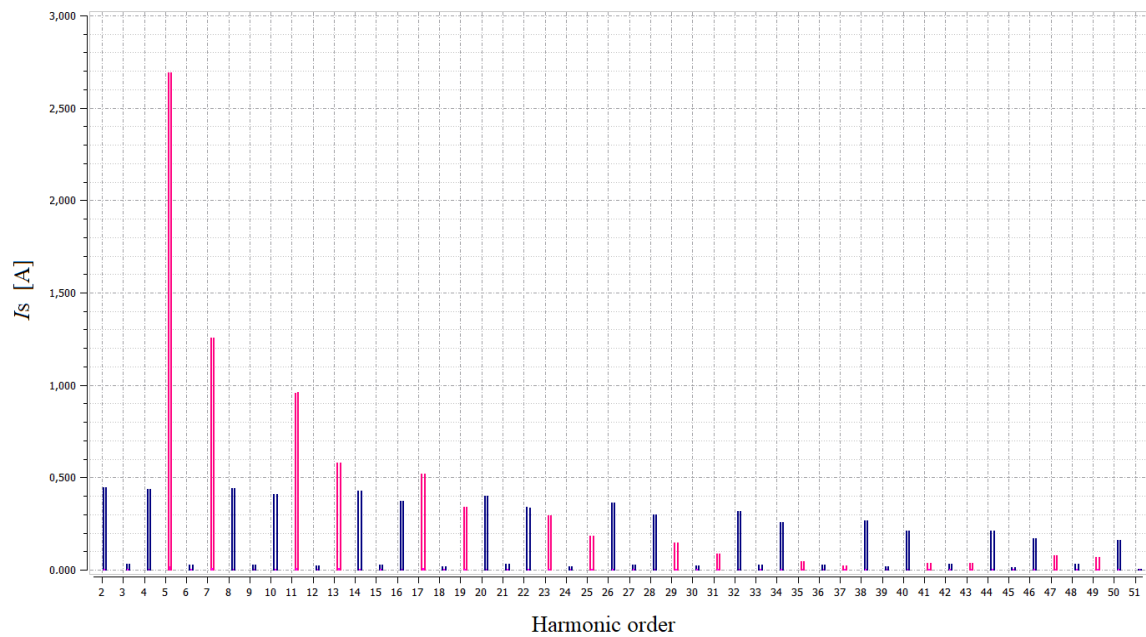

Figure 4.6   Example of grid current spectrum for $U_{CD} = 250$ V (the red manganese colour represents the characteristic harmonics)

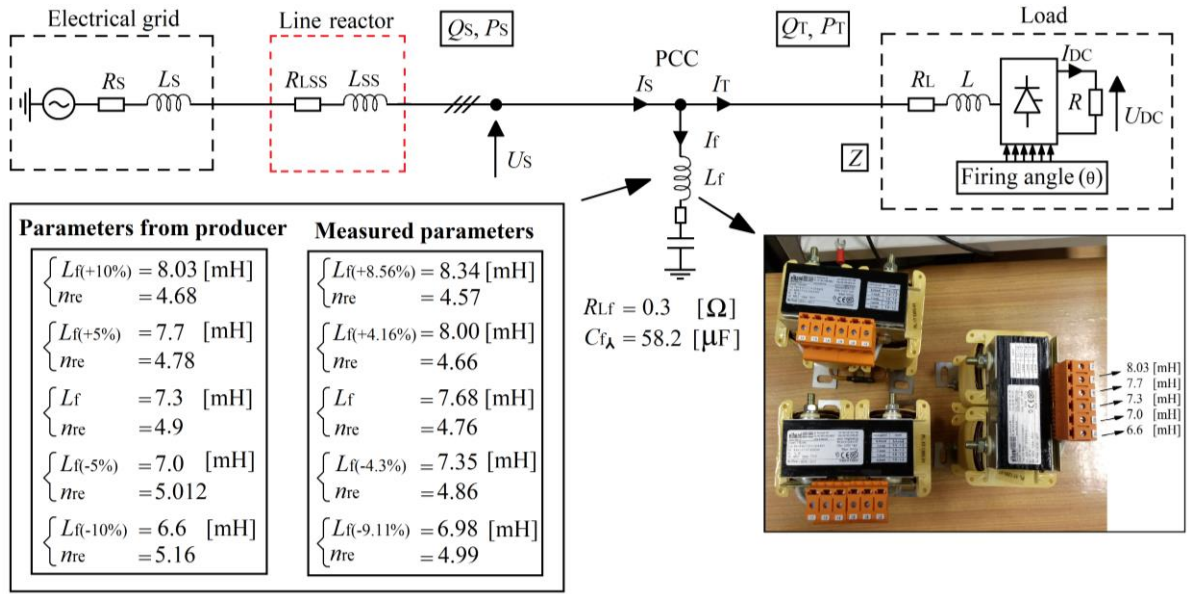### 4.1.1 Example of investigation performed on the PHF topologies: the detuning phenomenon

Figure 4.7   Power system equivalent circuit with filter reactor parameters

The PHF detuning phenomenon is investigated through the single-tune filter. It is performed by increasing or decreasing the filter resonance frequency in the goal to observe its behaviour regarding the harmonic to be eliminated and higher order harmonics as well.

It has been theoretically demonstrated during the simulation studies that the single filter efficiency is reduced on the mitigation of harmonic to be eliminated (e.g. 5th) when its resonance frequency is lower and fare from the frequency of that harmonic and that the amplification of 5th harmonic amplitude can occur when the filter is tuned to the frequency higher than the 5th harmonic frequency because of the parallel resonance. These laboratory investigations are just to confime the simulation studies.

The single-tuned filter presented in Figure 4.7 (laboratory model) is tuned for the investigation on the frequencies lower than the frequency of the 5th harmonic (measured paramters - Figure 4.8(b)).

Figure 4.8 presents the filter impedance versus frequency characteristics obtained from the simulation (Figure 4.8(a) - expected characteristics based on the manufacture parameters) and measured in the laboratory (Figure 4.8(b)). The different observed between data and characteristics in the both figures is due to the filter parameters tolerance.

The following laboratory data are recorded by taking as example the rectifier DC voltage (U_{DC}) equal to 250 V ($\theta = 62.54°$). For each tuning frequency the power system data were registered. The fundamental harmonic active and reactive power measured in the laboratory model at the grid side, filter terminals and rectifier input are presented in Table 4.1.

The grid voltage and current waveforms and spectrums are presented in Figure 4.9 and the filter current and rectifier input current waveforms and spectrums are presented in Figure 4.10. The grid voltage and current THD and the filter effectiveness are respectively presented in Figure 4.11 and Figure 4.12

Observing Figure 4.9, it can be seen that the lowest value of the 5th harmonic amplitude (the lowest THD as well - Figure 4.11(a)) in the grid voltage spectrum is obtained when the filter is tuned to the frequency of harmonic order 4.99, whereas in the case of grid current spectrum, the filter tuned to the frequency of 4.66 has the lowest 5th harmonics amplitude as well as the lowest THD (Figure 4.11(b)). By increasing the filter tuning frequency from n_{re} equal to 4.57 to n_{re} equal to 4.99, the grid current 5th harmonic amplitude should be decreasing

as the 5th harmonic amplitude observed in the grid voltage spectrum. This difference is due to the 5th harmonic current flowing from the grid side to the laboratory model.

The single-tuned filter efficiency presented in Figure 4.12 shows that the filter is more efficient on the 5th harmonic mitigation when its resonance frequency is on the harmonic order of 4.66, which is contrary to what can be observed in the characteristics of Figure 4.8(b).

According to the filter impedance versus frequency characteristics of Figure 4.8(b), the filter tuned to the frequency of 4.57 should present the highest 5th harmonic amplitude for both grid current and voltage and the filter tuned to the frequency of 4.99 should presents the lowest 5th harmonic amplitude for both grid current and voltage. But the reduction of the 5th harmonic amplitude in the grid current as presented in Figure 4.9 does not follow that principle because of the harmonics current flowing from the grid side.
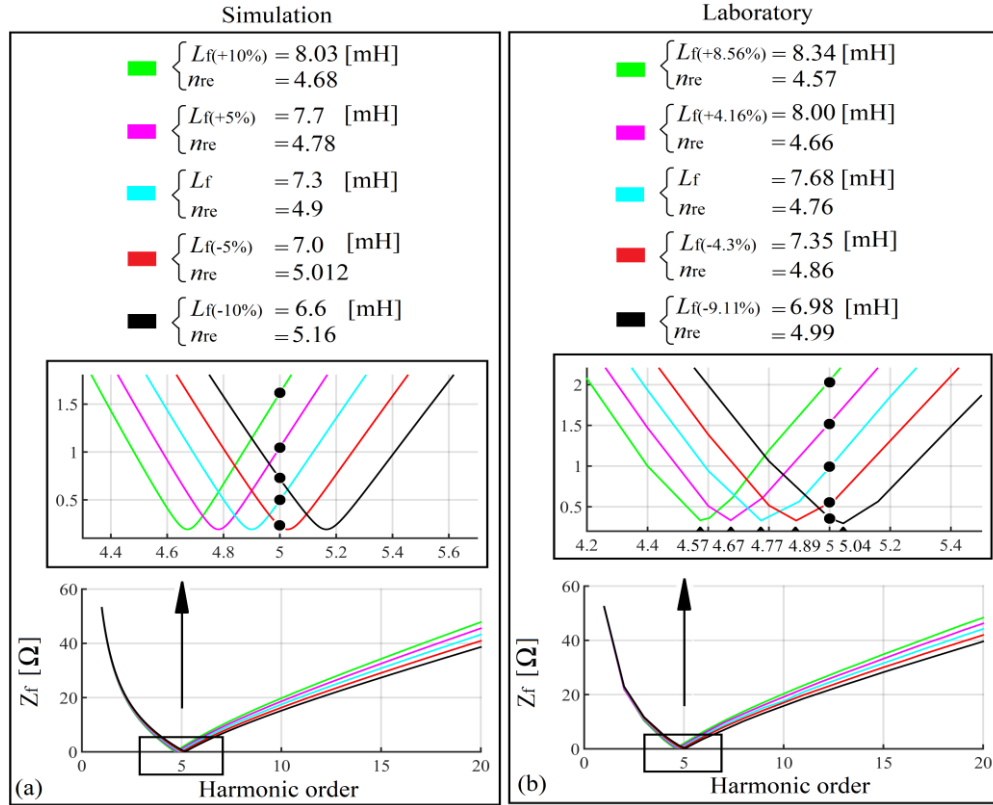

Figure 4.8   Filter impedance versus frequency characteristics: (a) expected characteristics from simulation and (b) characteristics measured in the laboratory

Table 4.1   Fundamental harmonic active and reactive power measured in the laboratory model

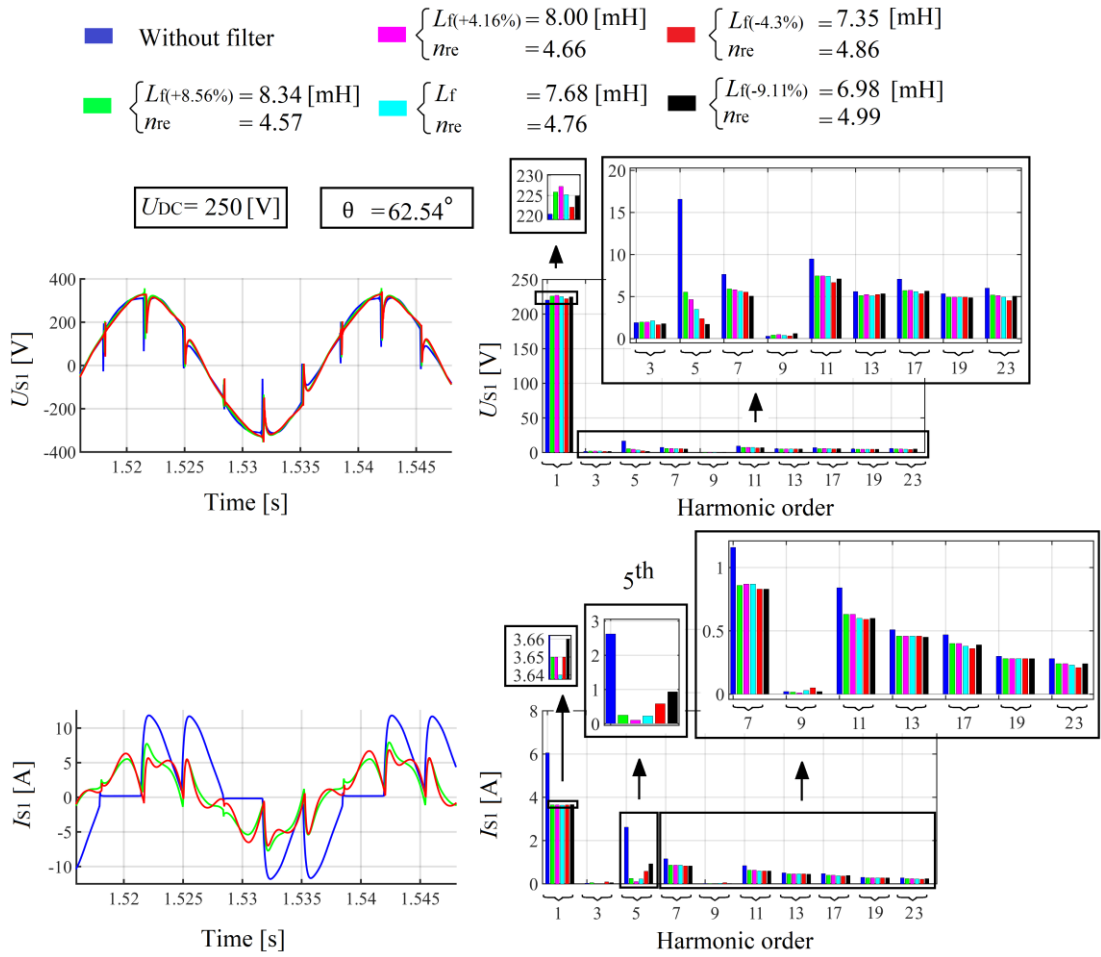| n_{re}	$P_{S1(1)}$ [W]	$Q_{S1(1)}$ [Var]	$P_{f1(1)}$ [W]	$Q_{f1(1)}$ [Var]	$Q_{T1(1)}$ [Var]
No filter connected	806.29	1065.6	-	-	-
4.57	821.66	83.81	16.99	-981.84	1067.4
4.66	826.15	83.53	16.10	-991.20	1076.4
4.76	815.84	83.21	16.90	-971.23	1056.1
4.86	807.39	94.73	16.10	-943.33	1039.5
4.99	819.69	78.11	17.46	-965.52	1045.1

Figure 4.9   Point of common coupling voltage and current waveforms and spectrums

The reactor and capacitor parameters tolerance has an influence on the PHF tuning frequency as well as on its work efficiency, therefor it is important to verifier the reactor and capacitor parameters after their reception from the producer. This varication should be based on the search of the filter parameters, which are close to the expected parameters. The investigations have also shown that the harmonics contains in the electrical grid flows through the filter, mostly those with frequencies close to the filter resonance frequency. The filter efficieny depends upon the electrical grid impedance and that dependency can be reduced be adding the line reactor between the filter and the PCC. The line reactor presence does not only mitigates the current harmonics amplitude flowing from the electrical grid, but it increases also the grid voltage distortion.
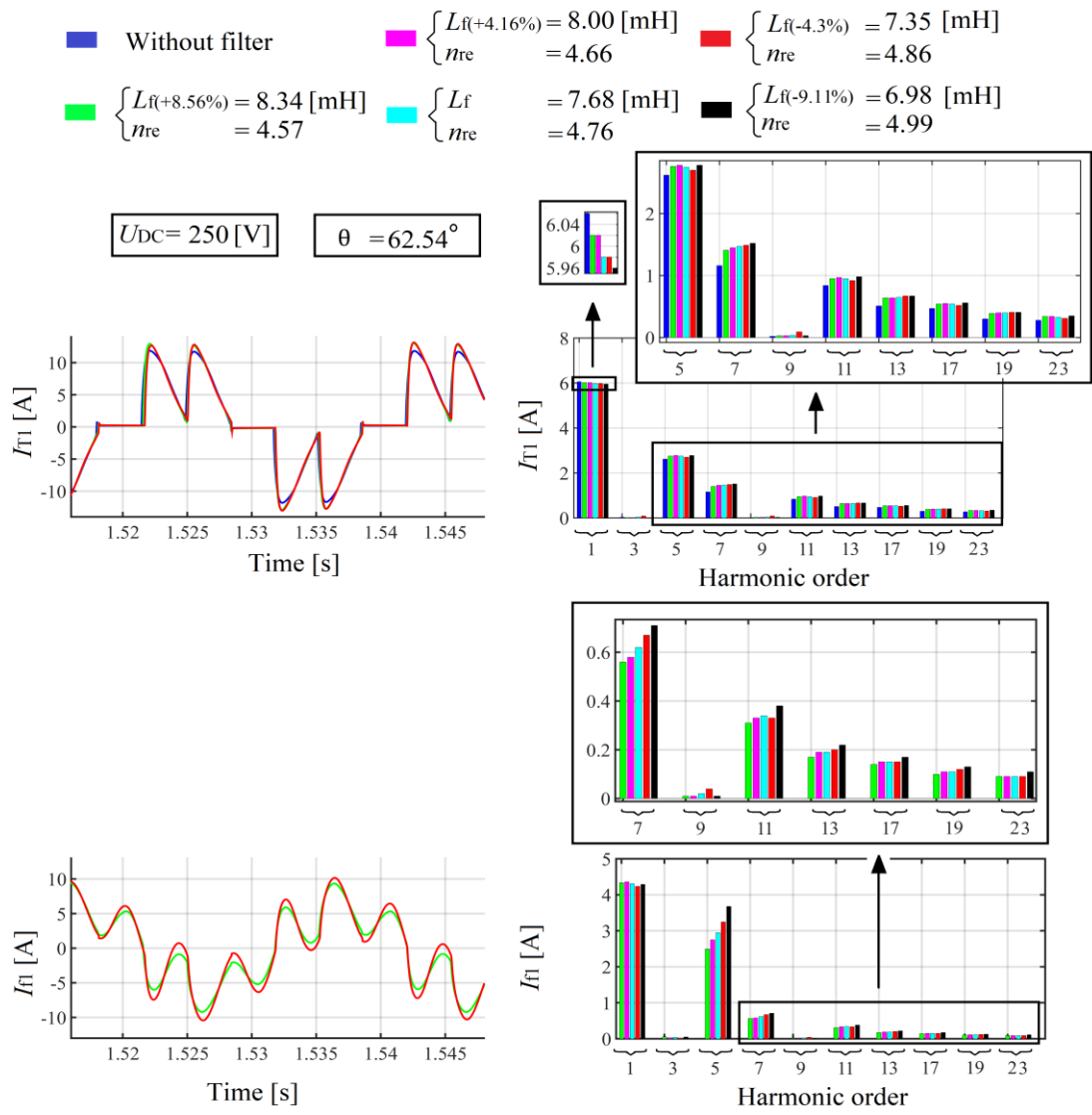
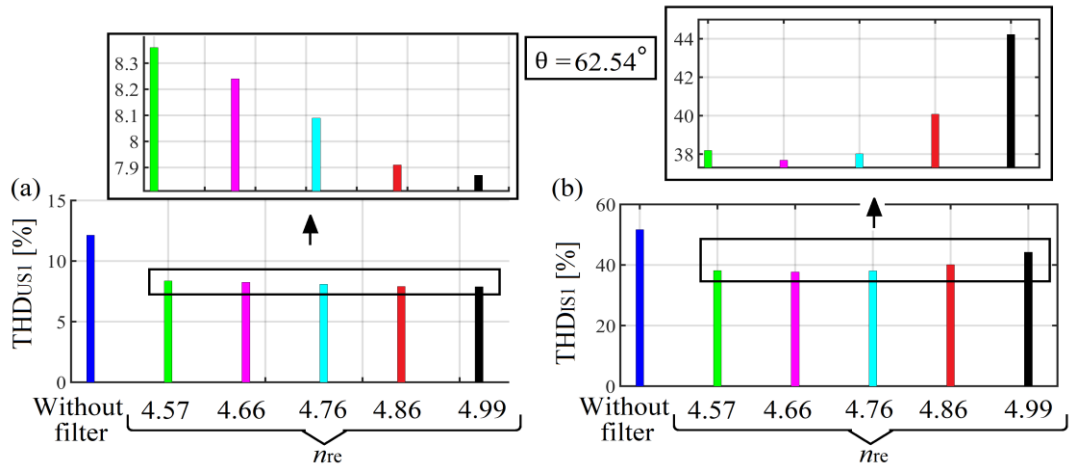Figure 4.10   Input rectifier and filter current waveforms and spectrums

Figure 4.11   Grid voltage and current THD for different resonance frequency
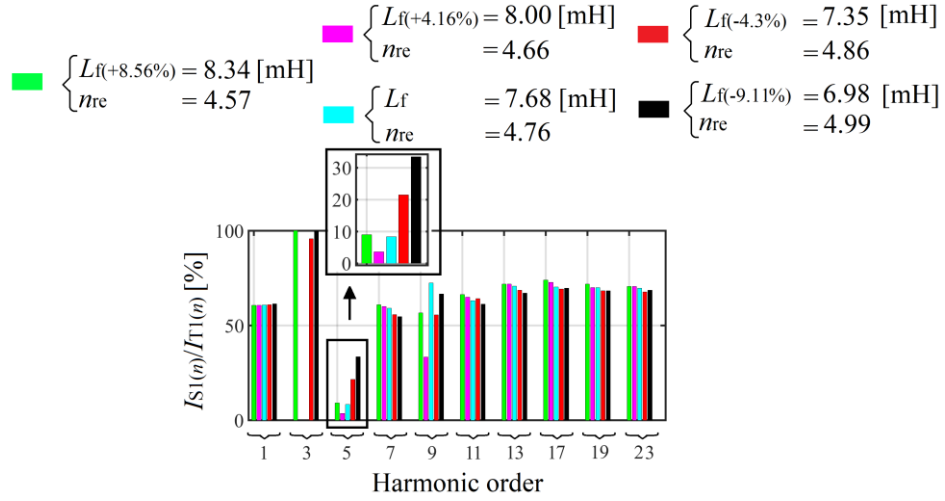
$\begin{cases} L_{f(+8.56\%)} = 8.34 \text{ [mH]} \\ n_{re} = 4.57 \end{cases}$ $\begin{cases} L_{f(+4.16\%)} = 8.00 \text{ [mH]} \\ n_{re} = 4.66 \end{cases}$ $\begin{cases} L_{f(-4.3\%)} = 7.35 \text{ [mH]} \\ n_{re} = 4.86 \end{cases}$ $\begin{cases} L_f = 7.68 \text{ [mH]} \\ n_{re} = 4.76 \end{cases}$ $\begin{cases} L_{f(-9.11\%)} = 6.98 \text{ [mH]} \\ n_{re} = 4.99 \end{cases}$

Figure 4.12   5th harmonic reduction efficiency
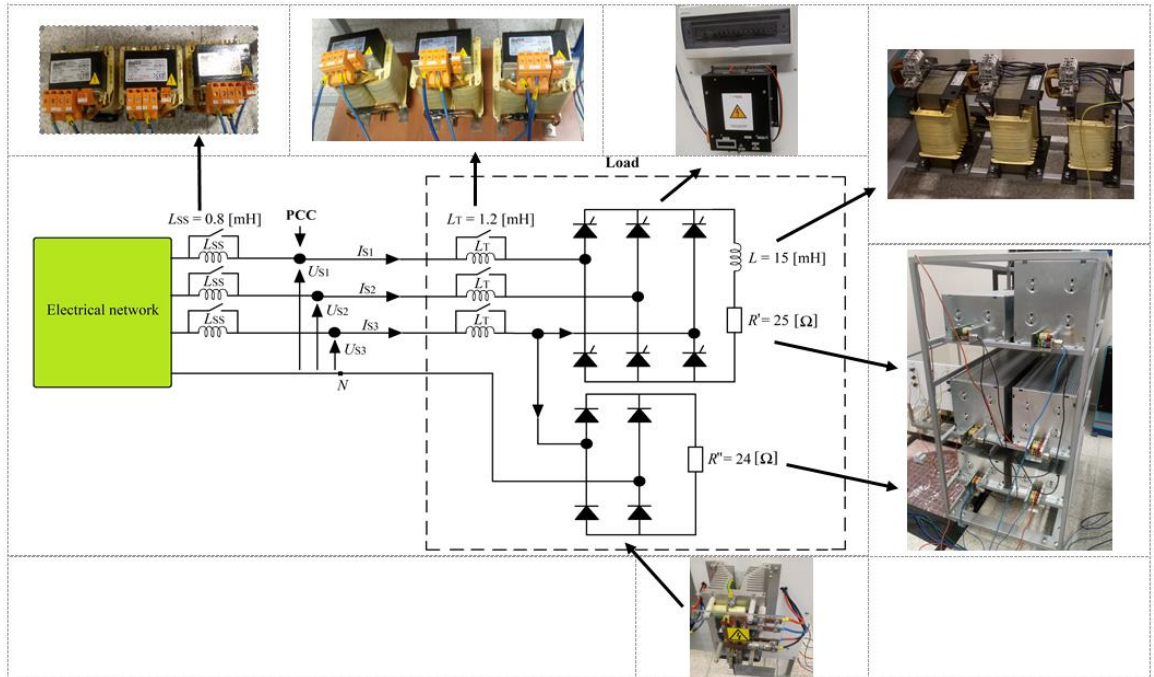
4.2   Shunt active power filters

Figure 4.13   Equivalent circuit of the laboratory model with components

The laboratory model equivalent circuit in which the SAPF was investigated is presented in Figure 4.13. The load is composed of three-phase thyristor bridge with resistance R and reactor L at its DC side and reactor L_T at its AC side. The one-phase diode bridge with 24 Ohm resistance at the DC side is used to obtain the current asymmetry. The investigated SAPF presented in Figure 4.14 is connected at the PCC.

The laboratory experiments are not focused on the design of the SAPF with its control system, but on the influence of the rectifier commutator reactor (L_T) and line reactor (L_{SS}) (see Figure 4.13) on the SAPF performances.

4.2.1   Example of studies performed on the SAPF

The Studies are about the influence of thyristor bridge input reactor influence on the SAPF performance.

The measured grid voltage and current spectrums and waveforms before the SAPF connection (L_{SS} and L_T are not connected) is presented in Figure 4.15. It can be seen in that

figure the PCC voltage and current distortion, the current asymmetry and the high level of fundamental harmonic reactive power.

Three cases of study based on the rectifier input reactor change (L_T) were considered after the SAPF connection: L_T – is not connected, $L_T = L_{\_inv} = 2$ mH and $L_T = 2.5$ mH $> L_{\_inv} = 2$ mH. During the experiments, the grid side line reactor (L_{SS}) was not considered.

Figure 4.16(b)(c) in comparison to Figure 4.16(a) shows that when the inverter input reactor inductance is equal or lower than the rectifier input reactor inductance, the PCC voltage and current waveforms ripples at the commutation are better reduced by the SAPF.
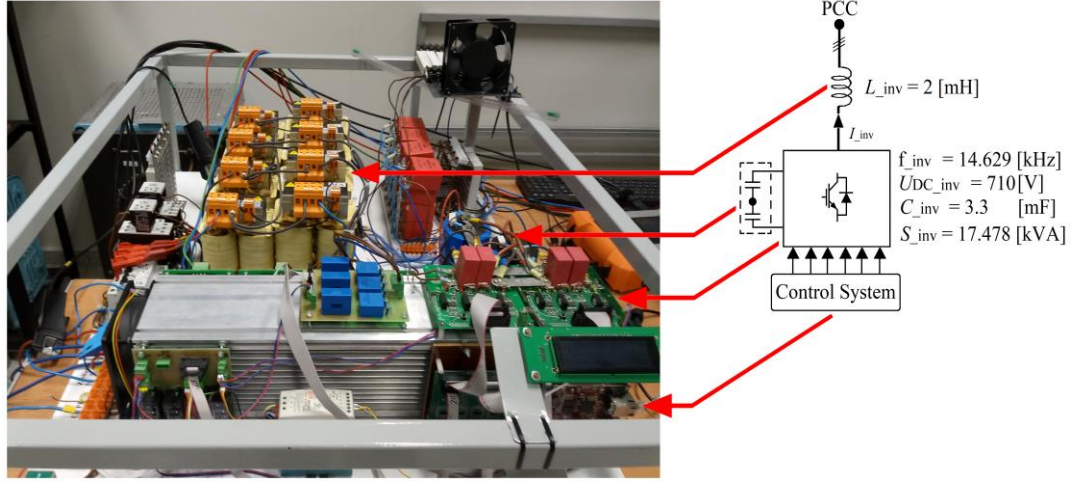

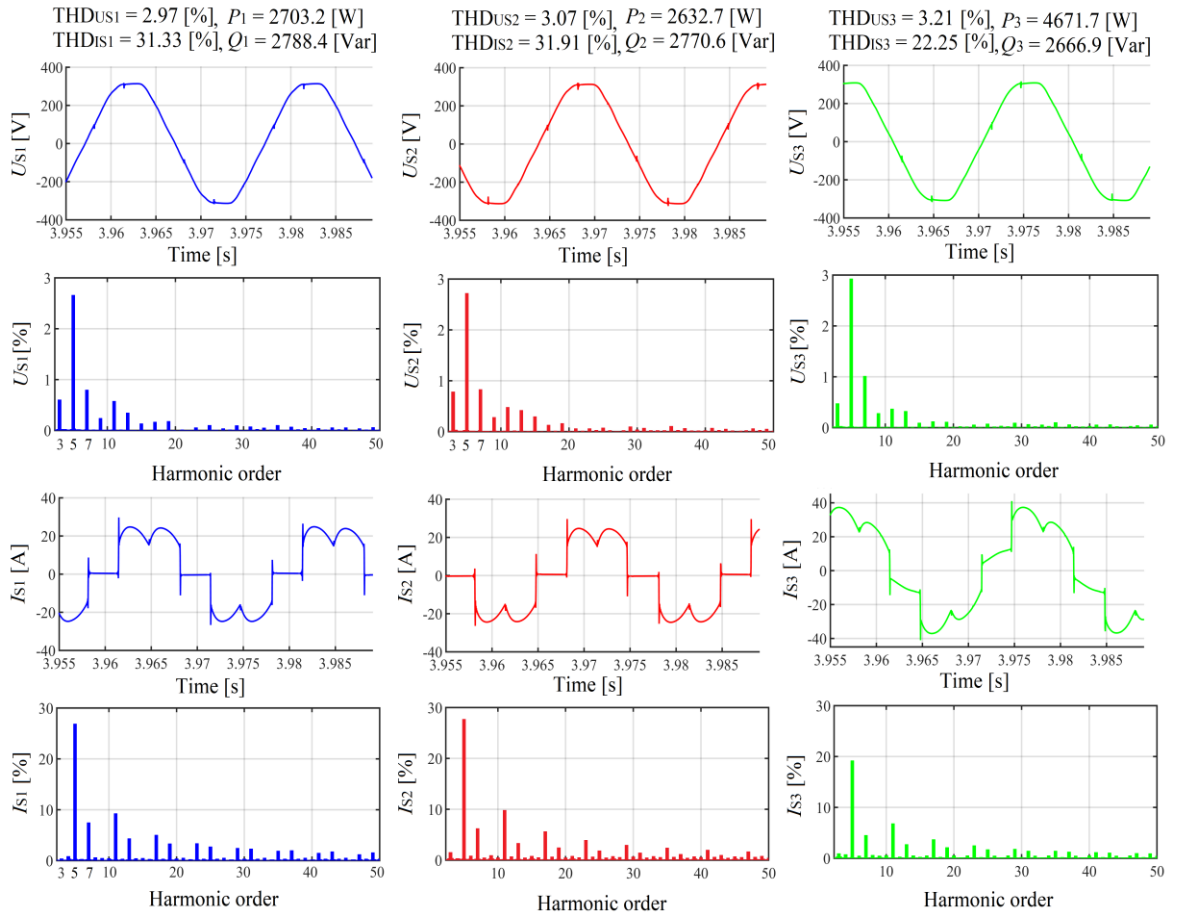Figure 4.14   Equivalent circuit of the laboratory model with components

Figure 4.15   Measured grid voltage and current waveforms with spectrums before the SAPF connection ($L_{SS} = L_T = 0$)
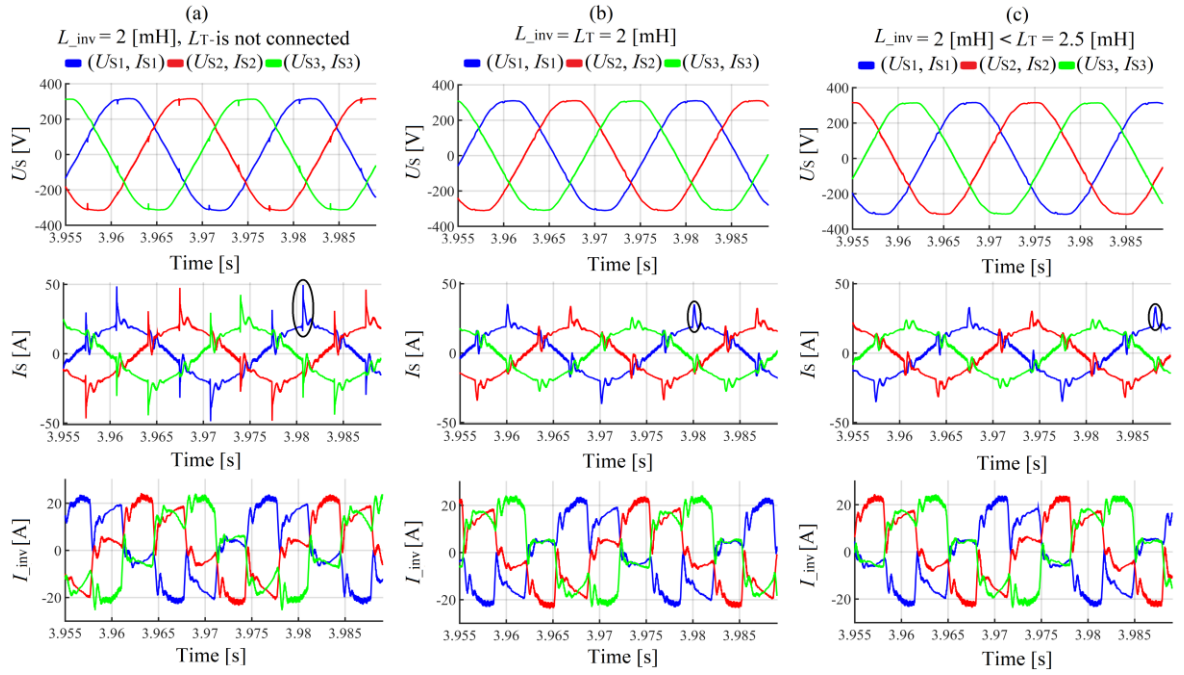
Figure 4.16 Comparison of grid voltage (U_S) and current (I_S) and SAPF current (I_{inv}) waveforms: (a) L_T is not connected, (b) $L_T = L_{inv} = 2$ mH and (c) $L_T > L_{inv}$
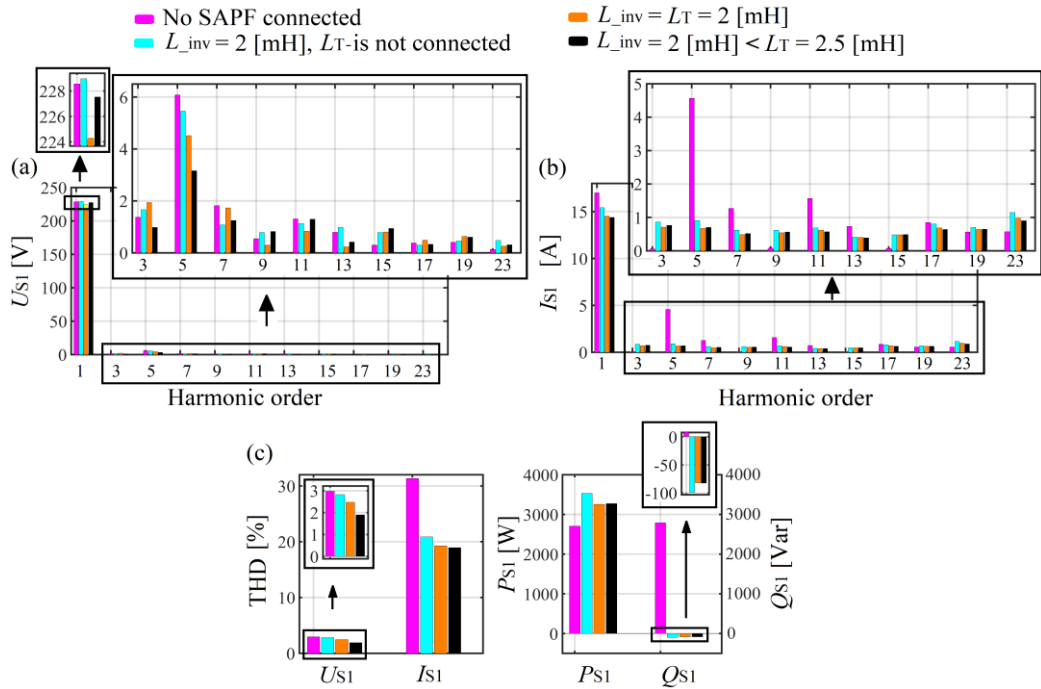

Figure 4.17 Comparison of: (a) PCC voltage spectrums, (b) PCC current spectrums and (c) PCC voltage and current THDs, active (P_1) and reactive powers (Q_1)

Figure 4.17 represents (for the three case studies) a comparison of PCC voltage and current spectrums and THD as well as the PCC active and reactive power. Only one-phase of each case is considered because of the PCC current balance after the SAPF connection. For L_{inv} equal or smaller than L_T, the PCC voltage and current 5th harmonic as well as THD are better mitigated (Figure 4.17(a) to (c)). It is important to notice that the PCC voltage contains harmonics, which can affect the results at the PCC.

The laboratory experiments have shown that:

− for a better reduction of grid voltage and current ripples at the commutation points of waveforms, the inductance of reactor (first-order filter) connected at the SAPF input for

switching ripples mitigation, should be smaller or equal to the inductance of the input rectifier reactor so called commutation reactor,

‒ when the SAPF with reactor at its input is connected at the PCC, the additional line reactor connection between the PCC and the grid is not recommendable, because the PCC voltage will be more distorted with inverter switching ripple.

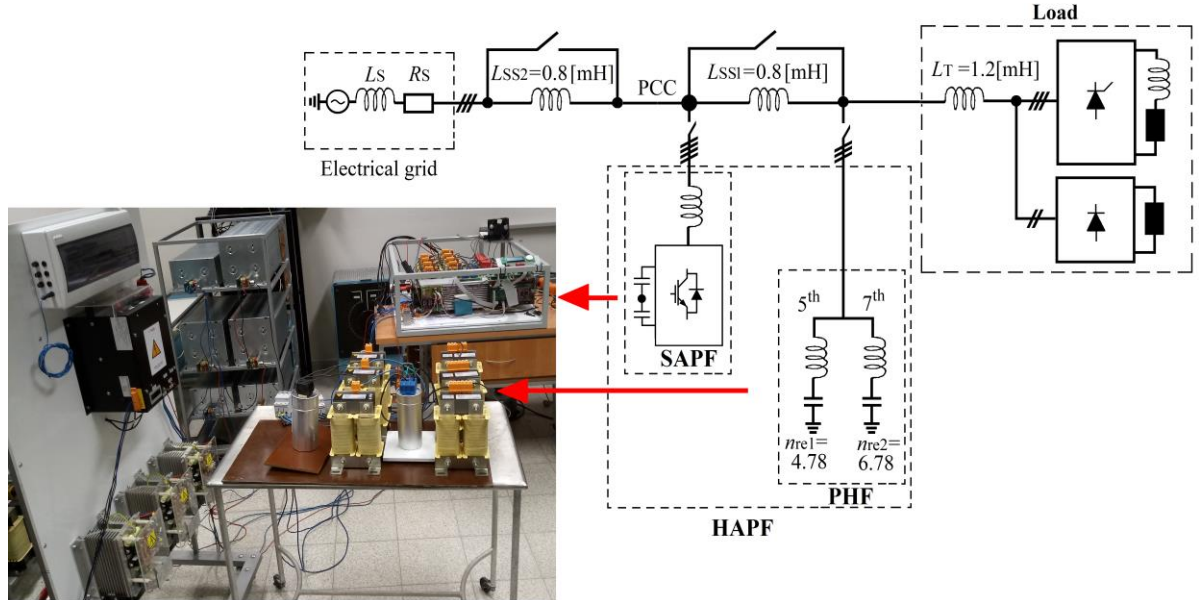## 4.3 Hybrid active power filter
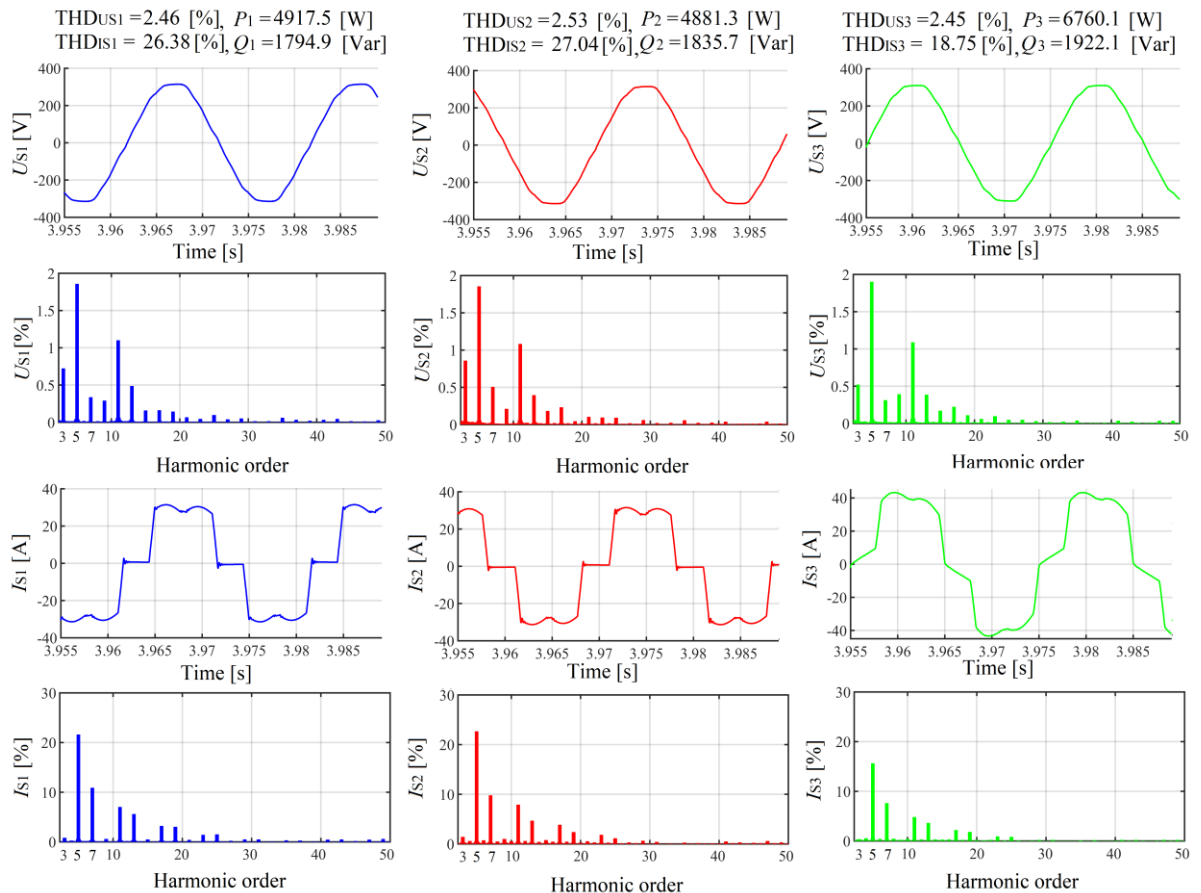

Figure 4.18   HAPF laboratory model

Figure 4.19   PCC voltage and current waveforms and spectrums measured when the HAPF is not connected (with L_T)

The model of HAPF presented in Figure 4.18 is an additional model of HAPF investigated in the laboratory. It consists of SAPF connected in parallel with the group of two single-tuned PHFs as presented in Figure 4.18. The PCC voltage and current waveforms and spectrums measured when the HAPF was connected, are shown in Figure 4.19.

4.3.1   Example of analysis performed on the HAPF

The analysis is about the connection and disconnection of the additional line reactor (L_{SS2} and L_{SS2}) in the power system. The HAPF is connected to the grid through the line reactor L_{SS2} (L_{SS1} disconnected) and the results are compared with those obtained when L_{SS1} (L_{SS2} not connected) was connected between the SAPF and the PHF group (Figure 4.18).

In the case where the HAPF has L_{SS1} connected between the SAPF and the PHF group (without L_{SS2}), the PCC current and voltage waveforms are less distorted (see Figure 4.20(a)).

The connection of the HAPF (without L_{SS1}) to the grid through the line reactor L_{SS2} presents the worst results in term of harmonics mitigation (Figure 4.21(a)-(c)) and fundamental harmonic reactive power compensation (Figure 4.21(d). The PCC voltage and current are more distorted because of the additional voltage drops on the line reactor L_{SS2} (Figure 4.20(b)) (The connection of L_{SS2} at the grid side has decreased the grid short-circuit power, increasing its impedance).

Connected between the filters (SAPF and the PHF group), the line reactor L_{SS1} helps on one hand, the group of PHF to mitigate the 5th and 7th current harmonics and on other hand, it helps the SAPF to mitigate the ripples at the commutation notches of grid voltage and current waveforms.

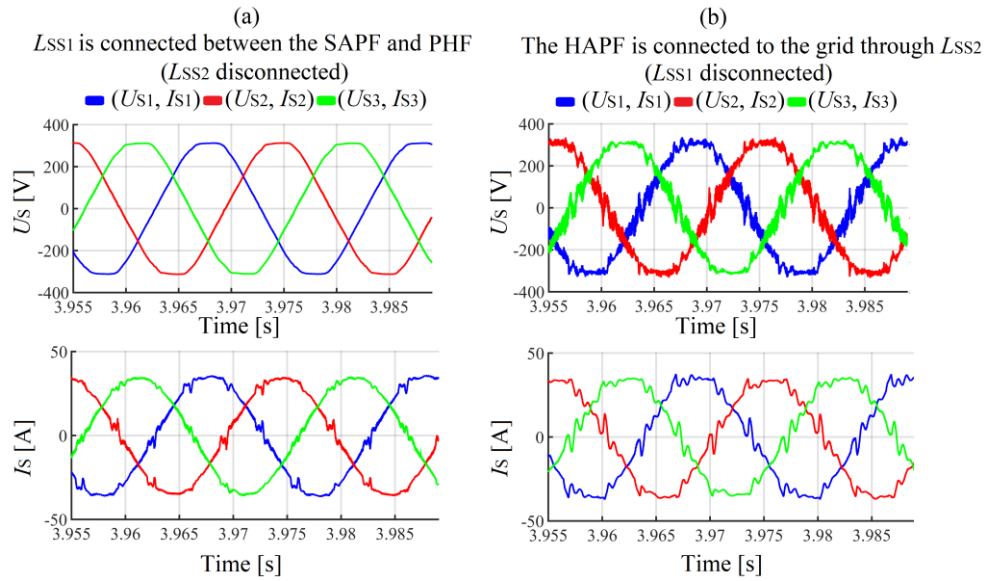

Figure 4.20   PCC voltage and current waveforms: (a) the line reactor L_{SS1} is connected between the SAPF and PHF (L_{SS2} disconnected) and (b) the HAPF is connected to the grid throught L_{SS2} (L_{SS1} disconnected)
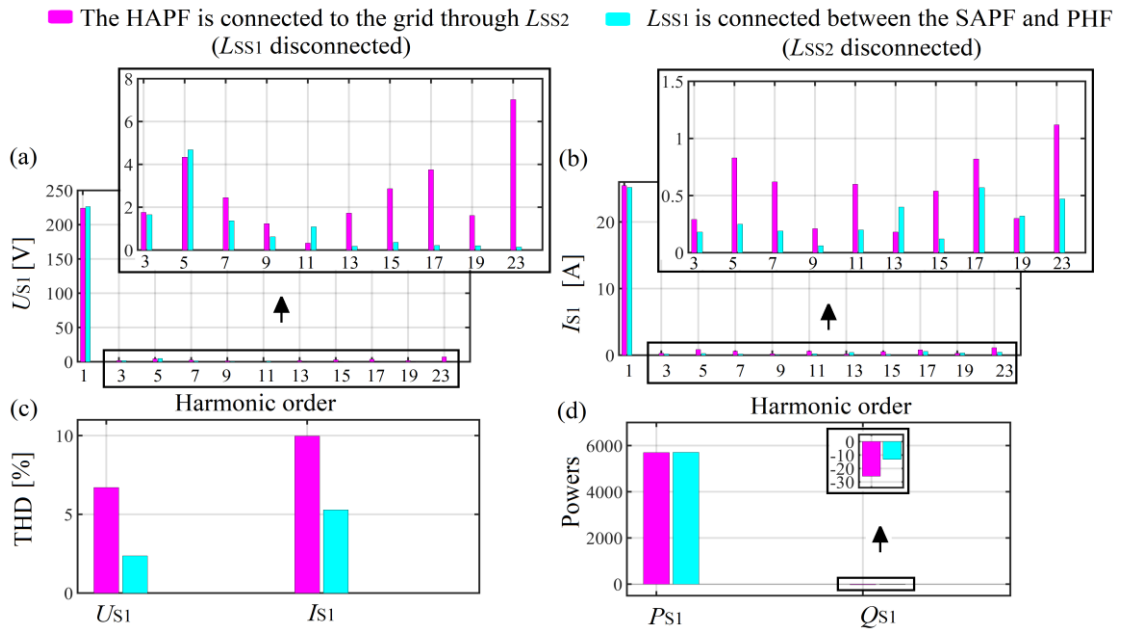
Figure 4.21   (a), (b) PCC voltage and current spectrums, (c) THD and (d) fundamental harmonic active and reactive powers

The laboratory experiments have shown that:
− the SAPF is better than the PHF in term of grid current harmonics mitigation,
− combined with the PHF (HAPF), the SAPF demants less power than when it is operating alone,
− the connection of the SAPF or HAPF to the PCC through a line reactor is not recommendable,
− in the configuration of HAPF where the SAPF and PHF are connected in parallel, if the PHF presents higher impedance of harmonic(s) to be mitigated than in the grid side, the line reactor between the SAPF and PHF is needed.

5. Conclusion

The thesis objective focused on the hybrid active power filter (HAPF) which is the combination of active power filter (APF) and passive harmonic filter (PHF). To achieve the thesis objective, the author performed different studies (simulation and laboratory) on the selected PHF and SAPF structures.

The acquired knowledge from the studies of the PHF and SAPF structures allowed the author to design and analyzed the hybrid active power filter (HAPF) structures: model of SAPF (three legs three wires) connected in series with the single-branch filter (simulation) and model of SAPF (three legs four wires) connected in parallel with the group of two single-branch filters (laboratory).

5.1   Simulation study results

The following PHF structures were considered: the single-tuned filter, the series PHF, the double-tuned filter, the broad-band filters (first, second, third-order and C-type filter) and Hybrid passive harmonic filter (HPHF). The author analyzed the PHF topologies basing on their impedance versus frequency characteristics, detuning phenomenon (due to the filter elements parameters (LC) change over the time or due to fault or atmospheric conditions), and damping resistance. All the quoted elements have an influence on PHF filtration efficiency. The comparison of some PHF structures (group of two single-filters & double-tune filter, series PHF & HPHF) as well as the methods of sharing the total reactive power in the filter group were also considered. The structures were tested as a stand-alone device as well as a part of the entire system including non-linear load and supply network with its internal equivalent impedance.

Basing on the impedance versus frequency characteristics, the author showed that the variation of the series PHF parameters decreases its efficiency on the harmonic to be blocked. Connected between the PCC and the rectifier load, it can be the source of harmonics amplification at the grid side. The disadvantages (e.g. harmonics amplification etc.) of the series PHF can be overcome by the shunt PHF (HPHF).

The author demonstrated that:

- the shunt PHFs (single-tuned, double-tuned and broad-band filters) should by tuned to the frequency a bit lower than the frequency of harmonic to be eliminated because of the aging of their elements (*LC*) which can caused the filter detuned. The harmonic to be eliminated should be the load (e.g. rectifier) characteristic harmonic after the fundamental harmonic. The bad choice of the shunt PHF resonance frequency can cause the amplification of harmonics at the electrical grid side and filter terminals,
- the increase of single-tuned filter resistance reduces its efficiency on the mitigation of harmonic to be eliminated at the grid side and increases its power losses,
- the filter group (two single-tuned filters) in comparison to the double-tuned filter (the same fundamental harmonic reactive power, reactor quality factor and voltage at their terminals) presentes higher value of inductances (more expensive in practice) and lower impedance for harmonics higher than the harmonics to which it is tuned,
- the first-order filter designed for the fundamental harmonic reactive power compensation, in the electrical power system with distorted voltage and current, can be a source of harmonics amplification (at the grid side),
- the second-order, third-order and C-type filter efficiency depends upon the choice of the damping resistance value. They can be the source of harmonics amplification (mostly the

characteristic harmonics near the fundamental) at the grid side if the damping resistance is not well chosen. Depending on their damping resistance value, they are better on the reduction of harmonics in wide band than the single-tune filter (grid side),

- the single-tuned filter compared to the broad-band filters (equal fundamental reactive power, equal reactor quality factor, and equal resonance frequency) and regardless of damping resistance value, is better on the mitigation (grid side) of harmonic which the frequency is near its resonance frequency,
- the second-order filter in comparison to the single-tuned filter and other the broad-band filters (equal fundamental reactive power, equal reactor quality factor, and equal tuning frequency) and regardless of damping resistance value, present higher power losses,

Six methods (Method A to F) of sharing the total fundamental reactive power in the filter group were presented and compared in this work. Despite the fact that the efficiency of filters whose individual components have been selected by different methods is very similar, method A (equal reactive for filters in the group) remains more attractive than other method because it demands less caculation and presents better resuls in term of filter group power losses.

The goal of designing the SAPF (three wires three legs structure) was to compensate the load fundamental harmonic reactive power, harmonics, and asymmetry and it was achieved using the original control algorithm – based on *p-q* theory - prosed by author. The influence of the line reactor (connected between the PCC and the grid side), rectifier input reactor and SAPF input reactor and DC capacitor on its efficiency, was also considered.

In the description of the *p-q* theory algorithm used in the SAPF control system, the author demonstrated that the distortion contained in the PCC voltage, if not filtred, affects the reference current and can be found in the grid current after compensation (the grid current waveform is then the replica of the PCC voltage waveform).

In the electrical system with rectifier load, the choice of the SAPF input reactor (*L*-filter) inductance value should be also based on the input rectifier reactor inductance value. It should be lower or equal to the input rectifier reactor inductance value for better mitigation of the grid current ripples at the commutation notches points. The connection of the line reactor between the PCC and the grid is not recommendable because of the PCC voltage distortion increased.

The analyzed HAPF was the topology of SAPF connected in series with the PHF (single-tuned filter). The goal of studying such of topology was to show that it is possible to reduce the power of SAPF (active part). The HAPF was applied to compensate the load fundamental harmonic reactive power and harmonics. The author demonstrated that the choice of the single-branch filter tuning frequency of that topology should not only depend on the rectifier (load to be compensated) characteristic harmonics but also on rectifier input reactor size. The author also proposed a control system algorithm based on *p-q* theory for that topology.

5.2   Laboratory study results

Basing on the investigations in the laboratory, the author demonstrated that the shunt PHFs efficiency depends upon the electrical grid impedance (the filter impedance of the harmonic to be eliminated should be smaller than the grid impedance of that harmonic), the supply voltage quality (with the distorted electrical grid voltage, after the filter connection, the harmonics flow from the grid to the filter (amplification of harmonics at the grid and filter side)) and the tolerance of the filter elements (*LC*). Before the shunt PHF design, the following infromations are needed:

- the load current characteristic harmonics and fundamental harmonic reactive power,
- the electrical grid estimeted impedance,
- the supply voltage spectrum at the PCC when the load to be compensated is not connected.

In the case of the distorted supply voltage (when the load to be compensated is not connected) and filter impedance of the harmonic to be eliminated not enaugh lower than the grid impedance of that harmonic, the author has demonstrated that the connection of the line

reactor between the grid and the PCC can be the solution with the disadvantage that the PCC voltage will be more distorted.

The author also demonstrated that after receiving the filter elements from the producer, it is important to verify (by measuring) if their parameters (reactor inductance and resistance, capacitor capacitance and resistance as well as filter resonance frequency) are within the tolerance or are the expected ones. The measured filter parameters can be a bit different from the nominal parameters because of the elements (*LC*) tolerance.

The investigation of the single-tune filter, group of two single-tuned filters, first and second-order filters in the laboratory confirmed the simulation studies.

The laboratory experiments of the SAPF were performed on the structure of four wires three legs with input reactors *L*. Based on that structure, the author presented the influence of the rectifier input reactor as well as the grid side line reactor on the SAPF efficiency (confirming the simulation).

The laboratory experiments of the HAPF were performed on the structure of SAPF (four wires three legs with *L* filter at the input connected in parallel with the group of two single-tuned filters. The author presented the advantages (the SAPF used less power) of that structure as well as the interest (improvement of the PHF efficiency) of connecting the line reactor between the SAPF and the group of PHF.

References

1   Azebaze M.C.S., Hanzelka Z., Mondzik A.: Different LC power filter topologies - effectiveness of reducing voltage distortion, International Conference on Renewable Energies and Power Quality, Spain, Madrid 4–6 May 2016.

2   Azebaze M.C.S., Hanzelka Z.: Hybrid power active filter – Effectiveness of passive filter on the reduction of voltage and current distortion, IEEE International Conference on Electric Power Quality and Supply Reliability, Estonia, Tallinn, 29-31 August 2016, pp.91-96.

3   Azebaze M.C.S., Hanzelka Z.: Passive harmonic filters. In Power quality in future electrical power systems, 1st ed Zobaa A.F., Shady H.E.A.A., IET the Institution of Engineering and Technology, London, United Kingdom, 2017, 77-127.

4   Czarnecki L. S., Ginn H.L.: The effect of the design method on efficiency of resonant harmonic filters, IEEE Transactions on Power Delivery, 2005, 20, 1, pp. 286-291.

5   Duarte L. H. S., Alves M. F.: The degradation of power capacitors under the influence of harmonics, IEEE on 10th International Conference on Harmonics and Quality of Power, 6-9 October 2002.

6   Elmathana M. T., Zobaa A. F., Abdel Aleem S. H. E.: Economical design of multiple-arm passive harmonic filters for an industrial firm-case study, IEEE 15th International Conference on Harmonics and Quality of Power (ICHQP), 17-20 June 2012.

7   Hanzelka Z.: Jakość energii elektrycznej: Część 4 – Wyższy harmoniczne napięć i prądów (c.d.), Twelve Electric, http://www.twelvee.com.pl/42767005.php?c=%D0%B5.

8   Klempka R., Hanzelka Z., Varetsky Y.: Bank harmonic filters operation in power supply system - cases studies, INTECH. 17 April 2013, Power Quality Issues, ed. Zobaa A. F, Rijeka INTECH, ISBN 980-953-307-532-2, pp. 201-23.

9   Micheal D., Nirod C.S.: On resonance and frequency response characteristics of electrical circuits, International Journal of Electrical Engineering Education, Manchester, October 2013, 50, 4, pp. 368–383.

10   Muhammad R., Muhammad I., Danang S.: Single tuned harmonic filter as total harmonic distortion (THD) compensator, CIRED, 23rd International Conference on Electricity Distribution, Lyon, June 15-18, 2015, p. 0056.

11   Sakar S., Abdel A. S. H. E., Balci M. E., Zobaa A. F.: A filter design approach to maximize ampacity of cables in nonsinusoidal power systems, IEEE International Conference, ISNCC 15-18 June 2015, Poland, Lagów, pp. 1-4.

12   Sakar S et al.: Optimal design of single-tuned passive filter using response surface methodology, IEEE International Conference, ISNCC, Łagow, Poland, 15-18 June 2015.

13   Zacharia P., Menti A., Zacharis Th.: Genetic algorithm-based optimal design of shunt compensators in the presence of harmonics, Elsevier, Electric Power Systems Research, April 2008, 78, pp. 728-735.

14   Abu-Rubu H., Iqbal A., Guzinski J.: High Performance Control of AC Drives with MATLAB/SIMULINK Models. John Wiley & Sons, Chichester, United kingdom, 2012.